Title	Nonlinear analytical modeling and characteristic analysis of symmetrical wire beam based composite compliant parallel modules for planar motion
Authors	Hao, Guangbo;Kong, Xianwen
Publication date	2014-07
Original Citation	Guangbo Hao, Xianwen Kong (2014) 'Nonlinear analytical modeling and characteristic analysis of symmetrical wire beam based composite compliant parallel modules for planar motion'. Mechanism and Machine Theory, 77 :122-147. doi: 10.1016/j.mechmachtheory.2014.02.012
Type of publication	Article (peer-reviewed)
Link to publisher's version	http://www.sciencedirect.com/science/article/pii/S0094114X14000500 - 10.1016/j.mechmachtheory.2014.02.012
Rights	Copyright © 2014 Elsevier Ltd. All rights reserved. NOTICE: this is the author's version of a work that was accepted for publication in Mechanism and Machine Theory. Changes resulting from the publishing process, such as peer review, editing, corrections, structural formatting, and other quality control mechanisms may not be reflected in this document. Changes may have been made to this work since it was submitted for publication. A definitive version was subsequently published in Mechanism and Machine Theory, [Volume 77, July 2014, Pages 122–147] DOI http://dx.doi.org/10.1016/j.mechmachtheory.2014.02.012
Download date	2024-05-14 10:23:07
Item downloaded from	https://hdl.handle.net/10468/1526

Nonlinear analytical modeling and characteristic analysis of symmetrical wire beam based composite compliant parallel modules for planar motion

Guangbo Hao[a,1], Xianwen Kong[b]

[a] *School of Engineering, University College Cork, Cork, Ireland.*
[b] *School of Engineering and Physical Sciences, Heriot-Watt University, Edinburgh, EH14 4AS, UK.*

ABSTRACT

This paper mainly deals with the nonlinear analytical modeling and characteristic analysis of two types of composite multi-beam modules for planar motion to enable rapid analysis and design synthesis. Each type of composite multi-beam module consists of identical, uniform and parallel wire beams, distributing uniformly along circle(s), with symmetrical cross sections. Analytical models of basic multi-beam modules with all beams uniformly spaced around a circle are firstly revisited. Analytical and nonlinear load-displacement equations are derived for the composite multi-beam modules, each of which is composed of two basic multi-beam modules with the same type connected either serially or in parallel. Finite element analysis (FEA) is carried out to compare and verify the analytical models. Detailed characteristic analysis and comparisons are conducted to compare three types of compliant six-beam modules whose twisting rotations are well constrained. These analytical results are capable of capturing some key quantitative nonlinear characteristics, such as kinematic effects, load-stiffening effect and nonlinear twisting stiffness (torsional stiffness), and can promote the design and analytical modeling of compliant parallel manipulators composed of compliant multi-beam modules. In addition, the nonlinear analytical models of other variations of parallel double multi-beam modules are derived.

Keywords: Compliant mechanisms; Composite modules; Symmetrical wire beams; Planar motion; Analytical modeling; Characteristic analysis

1. Introduction

   Compliant mechanisms (also flexure mechanisms) transmit/transform motions/loads by deformation of their compliant members/links, which possess positive stiffness or even zero stiffness and negative stiffness [1-3]. They have advantages including increased performance and reduced cost including eliminated backlash and friction, reduced wear and lubrication, and reduced number of parts (up to a monolithic configuration), and have therefore been extensively used in a variety of applications such as a high-precision manipulator [4], a vibratory bowl feeder [5] and a compliant assembly system device [6].

   Recently, wire-beam based compliant mechanisms/modules have drawn much attention from researchers. For example, a number of synthesis works have been reported in [7-13], spatial 3-DOF translational compliant parallel manipulators composed of only identical wire-beam based compliant mechanisms have been proposed in [14-15], and nonlinear analysis/modeling and mobility analysis have been presented in [16-18]. This paper is limited to a class of wire-beam based compliant modules with planar motion (two translations and one rotation) as the primary motion, which is composed of identical, uniform and parallel wire beams with symmetrical cross sections. For convenience, this class of wire-beam based compliant module refers to the *compliant multi-beam module* throughout this paper, which has the following potential applications/merits.

   (a) The compliant multi-beam module can be fabricated using the carbon nanotubes (CNTs). This may lead to novel CNT-based compliant mechanisms [19-21] used in the emerging nano-electro-mechanical-systems (NEMS).

   (b) The compliant multi-beam module may act as a standalone motion stage actuated by the non-contact electromagnetic actuators [17]. This motion stage has a very simple configuration and large out-of-plane stiffness, and has no heat effect from the electromagnetic actuator due to the non-contact actuation. Due to the fact that the output stage acts as the input stage as well, no lost motion exists and fewer sensors are needed.

   (c) Compliant multi-beam modules can also be used as compositional units of new multi-axis compliant parallel manipulators, for example as a spatial leg to enhance the out-of-plane stiffness of an XY compliant parallel manipulator [22], and as a passive PPR joint of an XYZ compliant parallel manipulator [14-15] (see Fig. 1 for example). Here, P and R represent prismatic joint and revolute joint, respectively. This compliant multi-beam module offers an alternative to produce multi-axis compliant parallel manipulators instead of using leaf-beam or lumped-compliance joints [23, 24], and has larger out-of-plane stiffness than them.

   (d) A simpler and more accurate analytical model can be derived for the compliant multi-beam module since the 3D modeling of wire beams is easier and better developed [16, 25-27] compared with the 3D modeling of the conventional lumped-compliance hinge/pivot and leaf/blade/sheet used in the modeling of the compliant joints [23, 24].

   (e) The compliant multi-beam module can provide large-range planar motion with well-constrained out-of-plane motion and does not produce very large primary motion stiffness. This enables the use of the voice coil actuator for large-range motion since a larger primary stiffness will require a bulkier voice coil actuator to produce higher peak force [14, 28].

   There are mainly three types of compliant multi-beam modules with regularly distributed wire beams, which have been mentioned in [16, 29], and further detailed below.

   The first type of compliant multi-beam module is a simple purely parallel mechanism, composed of a base, multiple identical and uniform parallel beams (beam number *n*>2) with symmetrical cross sections, and a motion stage. The base and

---

motion stage, which are both assumed to be rigid, are connected by the wire beams (Fig. 2a). Here, all the beams are uniformly spaced around a circle, *pitch circle*, of radius r_n on the base and on the motion stage. This type of compliant multi-beam mechanism is called the *basic multi-beam module* throughout this paper. A basic six-beam module is shown in Fig. 2a.

The other two types of compliant multi-beam modules are referred to the *composite multi-beam modules* throughout this paper, each of which is composed of two basic multi-beam modules with the same type connected either serially or in parallel. As shown in Figs. 2b and 2c, the second type is a hybrid mechanism, composed of two basic three-beam modules in series (Fig. 2b), i.e. one *serial double three-beam module*; and the third type is a purely parallel mechanism, composed of two basic three-beam modules in parallel with beams uniformly spaced around two circles (Fig. 2c), i.e. one *parallel double three-beam module*. Note that the second type (Fig. 2b) involves an uncontrollable/under-constrained secondary stage with internal in-plane DOFs (degrees of freedom).
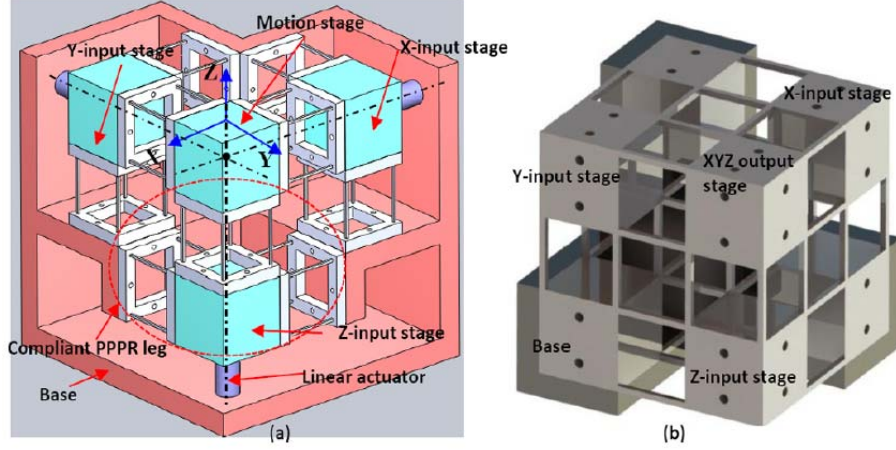

Fig. 1. A compact and decoupled XYZ compliant parallel manipulator composed of identical basic compliant four-beam modules: (a) a 3-PPPR XYZ compliant parallel manipulator, and (b) a corresponding monolithic design fabricated from a cubic material by three orthogonal directions' cutting.
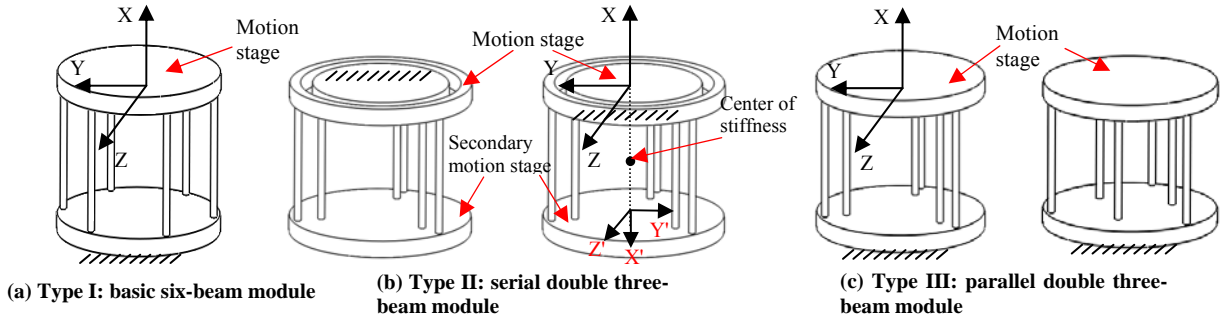

(a) Type I: basic six-beam module **(b) Type II: serial double three-beam module** **(c) Type III: parallel double three-beam module**

Fig. 2. Three types of compliant six-beam modules including basic and composite configurations

In comparison with finite element analysis (FEA) using commercial software, the analytical modeling for the compliant multi-beam modules in this paper enables rapid analysis and design synthesis, and provides exact analytical constraint models. Using the constitutive, compatibility and equilibrium conditions, Ref. [16] presented thorough theoretical solutions to the nonlinear load-displacement equations of the basic multi-beam modules using free body diagram method. Three nonlinear methods of increasing accuracy and complexity were proposed: an approximate analytical method, an improved approximate analytical method and a numerical method. The constitutive conditions for the single wire beam used in [16] are based on the assumption that the two bending deformations are decoupled or are weakly coupled irrespective of twisting moment. A more accurate analytical spatial beam constraint model for the single symmetrical wire beam was recently derived in [25, 26, and 30] without the above decoupling assumptions. However, due to the nature that the two bending angles are well constrained in the compliant multi-beam modules, the nonlinear models for the basic multi-beam modules proposed in [16] are as accurate as those obtained using the spatial beam constraint model proposed in [25, 26, and 30]. This can be verified by comparing the analytical models in [16] and general analytical models of basic multi-beam modules in [30, 31] using a nonlinear strain energy method, principle of virtual work (see Eqs. (6.73)－(6.75) in [30] and Eqs. (54)－(56) in [31] for example). Note that compared with the free body diagram method, the energy based method can reduce the number of unknown variables to only six via eliminating the internal load variables. However, the internal loads are desirable to be known in compliant mechanisms for estimating stress level etc. Also, due to the involved non-linearities it will be extremely complex to invert the relations to obtain displacements in terms of forces as demonstrated in [30], which is eventually desired in this paper.

Based on the above advances and under intermediate displacement range and Euler-Bernoulli-beam assumptions[2], this paper

---

[2]This article accounts for the non-linearity of load-equilibrium equations under the condition of intermediate displacement range where the transverse displacement is up to ±10% of beam length or the rotational displacement is up to ±0.1 radians [3]. Euler-Bernoulli-beam assumptions include: (1) Plane cross-sections remain plane (without warp effect) and perpendicular to the neutral axis in deformation; (2) The in-plane distortion of the plane cross-sections after deformation are neglected. Note that although ε_{yy} and ε_{zz}, caused by the principle strain σ_{xx} are not negligible due to the Poisson ratio. However, these presences don't affect the calculation of the end displacements of the slender beam because stresses σ_{yy} and σ_{zz} are both zero.

mainly studies on nonlinear analytical modeling of the two types of composite multi-beam modules, and then implements analytical characteristic analysis and comparisons of three types of compliant multi-beam modules. These works will contribute to the design and analytical modeling of standalone desktop-size XY motion stages [17] and translational compliant parallel manipulators [14, 15, and 22]

This paper is organized as follows. Section 2 revisits the previous work on basic multi-beam modules. In Section 3, the nonlinear and analytical load-displacement equations of composite multi-beam modules are investigated, and several typical analytical models are compared with FEA results. Section 4 analyzes and compares the characteristics of three types of compliant six-beam modules. Discussions are presented in Section 5. Finally, conclusions are drawn.

To simplify the derivations and make translational displacements and rotational angles (or forces and moments) comparable [18], all translational displacements and length parameters are divided by the beam length L, forces by EI/L^2, and moments by EI/L. Here, E and I denote, respectively, the Young's modulus and the second moment of the area of a symmetrical cross-section. For example, $I=\pi D^4/64$ for beams with round cross-section of a diameter D and $I=T^4/12$ for beams with square cross-section of a thickness of T. The normalized beam is equivalent to a beam with unit length, unit Young's modulus and unit cross-sectional moment. Throughout this paper, non-dimensional quantities are represented by the corresponding lower-case letters.

2. Basic Multi-Beam Modules Revisited

2.1. A basic three-beam module

The free body diagram of a basic three-beam module is shown in Fig. 3 [16]. All external loads, p (axial force), f_y, f_z (transverse forces), m_x (twisting moment), m_y and m_z (bending moments), can be regarded to act at the center, O', of the motion stage to cause the motion stage to move by deformation of the compliant beams. p, f_y and f_z are the forces along the X-, Y- and Z-axes, respectively; m_x, m_y and m_z are the moments about the X-, Y- and Z-axes, respectively. Here, the O-XYZ coordinate system is the global one. For the purpose of simplification, the gravity of the motion stage (including the payloads on it) is integrated into the axial force, and the weights of the compliant beams, which are very small, are neglected.
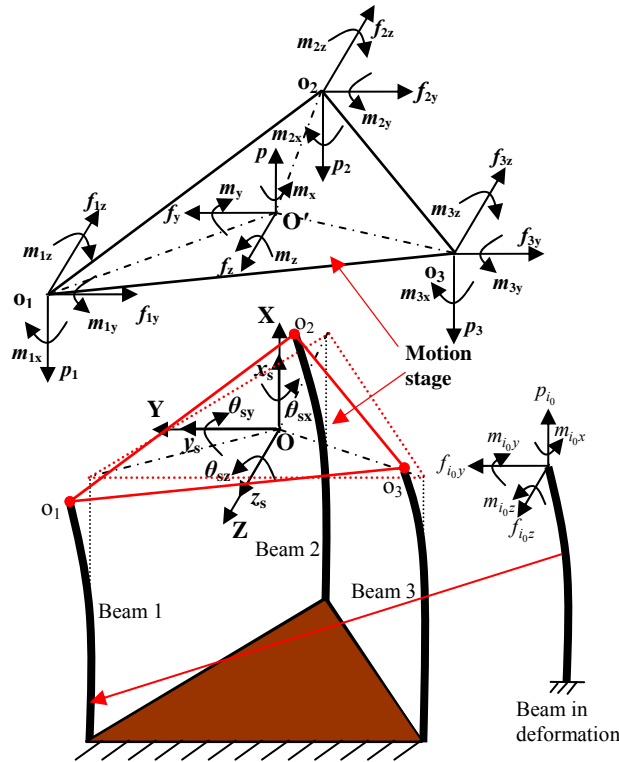

Fig. 3. Free body diagram of a basic three-beam module [16]

All translational displacements of the center, O', along the X-, Y- and Z-axes are denoted by x_s (axial displacement) y_s and z_s (transverse displacements), respectively. All rotational displacements (angles) of the motion stage about the X-, Y- and Z-axes are denoted by θ_{sx} (twisting angle), θ_{sy} and θ_{sz} (bending angles), respectively. In the basic three-beam module, the three out-of-plane motions are well suppressed, and its motion stage is constrained to move within the YZ plane, which leaves y_s, z_s and θ_{sx} as the three outputs (DOFs). Institutively, if the pitch-circle radius r_3 of the beams (accordingly the motion stage) becomes relatively large, the rotation of the motion stage about the X-axis will be constrained as well.

Note that, in the following sections for the compliant multi-beam modules: basic and composite, all loads and displacements shown in all the figures are represented by the non-dimensional quantities in the coordinate system O-XYZ unless indicated specifically otherwise, and the global coordinate system, loads and displacements are defined in a similar way to the basic three-beam module.

3

2.2. Nonlinear analytical models of basic multi-beam modules

Throughout this paper, we will use the approximate nonlinear analytical solutions (Eq. (1)) proposed in [16] for enabling characteristic analysis of basic multi-beam modules. These solutions offer a solid foundation for deriving analytical models of composite multi-beam modules since they are simple, analytical and accurate enough for most engineering applications especially if the twisting rotation and/or the bending moments can be very small.

$$
\begin{cases}
\theta_{sx} \approx \dfrac{m_x + (m_z z_s + m_y y_s)e}{n(\delta + ar_n^2 + per_n^2/n)} \approx \dfrac{m_x + (m_z f_z + m_y f_y)e/(na+pe)}{n(\delta + ar_n^2 + per_n^2/n)} \\[2mm]
y_s \approx \dfrac{f_y + m_y \theta_{sx} e}{na + pe} \\[2mm]
z_s \approx \dfrac{f_z + m_z \theta_{sx} e}{na + pe} \\[2mm]
\theta_{sy} \approx \dfrac{2}{nr_n^2}(\dfrac{1}{d} + y_s^2 r + z_s^2 r)[m_y + (nc + ph)z_s] - 2\theta_{sx} y_s i \\[2mm]
\theta_{sz} \approx \dfrac{2}{nr_n^2}(\dfrac{1}{d} + y_s^2 r + z_s^2 r)[m_z - (nc + ph)y_s] - 2\theta_{sx} z_s i \\[2mm]
x_s \approx \dfrac{p}{nd} + (y_s^2 + z_s^2)i + \dfrac{p}{n}(y_s^2 + z_s^2)r + r_n^2 \theta_{sx}^2 i + \dfrac{p}{n}r_n^2 \theta_{sx}^2 r + 2(y_s \theta_{sz} - z_s \theta_{sy})k - \dfrac{2}{n}(m_y y_s + m_z z_s)\theta_{sx} r
\end{cases} \tag{1}
$$

where $n=3$ or an even number greater than 3. The approximate displacements of the motion stage for a given set of loads are obtained in the sequence of (a) the twisting angle, θ_{sx}, (b) the two transverse displacements, y_s and z_s, (c) the two bending angles, θ_{sy} and θ_{sz}, and (d) the axial displacement, x_s.

Equation (1) can capture the desirable nonlinear characteristics such as buckling load ($p_{crit} = -10n$ if m_y and m_z are quite small), load-stiffening effects [16] attributing to the positive axial tensile force in the output equations (y_s, z_s and θ_{sx}), and the kinematic effects (including purely kinematic and elastokinematic) [16] in the DOC (degree(s) of constraint) equations (x_s, θ_{sy} and θ_{sz}). Some characteristics such as kinematic and load stiffening effects cannot be observed from linear analytical load-displacement equations [18] for the basic multi-beam modules. It can be observed that the twisting angle, θ_{sx}, is the dominant factor to couple the motion together. If $\theta_{sx}=0$, all motion equations can be largely simplified with two transverse motions independent of each other. Other stiffness characteristics (including the primary motion stiffness and the parasitic motion stiffness) will be detailed in the following sections in comparisons with other two types of composite multi-beam modules.

In Eq. (1) and throughout this paper, the non-dimensional numbers are defined as follows [16, 25, and 31]:

$a= 12, b= 4, c=-6$;

$d=16/(D/L)^2$ for round beams with diameter of D or $12/(T/L)^2$ for square beams with a thickness of T as examples;

$e= 1.2, g= 2/15, h=-0.1$;

$i=-0.6, j=-1/15, k= 1/20$;

$r= 1/700, s= 11/6300, q=-1/1400$;

$\delta=2G/E=1/(1+v)$ (G is the Shear Modulus, and v is the Poisson Ratio).

Based on the improved approximate analytical model in [16], more accurate analytical models of basic multi-beam modules can be obtained as follows.

$$
\begin{cases}
\theta_{sx} \approx \dfrac{m_x + (m_z \bar{z}_s + m_y \bar{y}_s)e}{n[\delta + ar_n^2 + per_n^2/n - (2ci + 2phi/n)(\bar{z}_s^2 + \bar{y}_s^2)] + (m_y \bar{z}_s - m_z \bar{y}_s)(2hi - e)} \\[2mm]
y_s \approx \dfrac{f_y + m_y \theta_{sx} e - m_z \theta_{sx}^2(h-1)e - (nc + ph)\bar{\theta}_{sz}}{na + pe} \\[2mm]
z_s \approx \dfrac{f_z + m_z \theta_{sx} e + m_y \theta_{sx}^2(h-1)e + (nc + ph)\bar{\theta}_{sy}}{na + pe} \\[2mm]
\theta_{sy} \approx \dfrac{2}{nr_n^2}[\dfrac{1}{d} + (y_s^2 + z_s^2 + r_n^2 \theta_{sx}^2 + r_n \theta_{sx} y_s)r][m_y + (nc + ph)z_s - m_z \theta_{sx}(h-1)] - 2\theta_{sx} y_s(i + \dfrac{p}{n}r) \\[2mm]
\qquad - \dfrac{2}{nr_n^2}[\dfrac{1}{d} + (y_s^2 + z_s^2 + r_n z_s)r][m_z + m_y \theta_{sx}(h-1)]\theta_{sx} + 2\theta_{sx}^2 z_s i \\[2mm]
\theta_{sz} \approx \dfrac{2}{nr_n^2}[\dfrac{1}{d} + (y_s^2 + z_s^2 + r_n^2 \theta_{sx}^2 - r_n \theta_{sx} y_s)r][m_z - (nc + ph)y_s + m_y \theta_{sx}(h-1)] - 2\theta_{sx} z_s(i + \dfrac{p}{n}r) \\[2mm]
\qquad - \dfrac{2}{nr_n^2}[\dfrac{1}{d} + (y_s^2 + z_s^2 - r_n z_s)r][m_y - m_z \theta_{sx}(h-1)]\theta_{sx} - 2\theta_{sx}^2 y_s i \\[2mm]
x_s \approx \dfrac{p}{nd} + (y_s^2 + z_s^2)i + \dfrac{p}{n}(y_s^2 + z_s^2)r + r_n^2 \theta_{sx}^2 i + \dfrac{p}{n}r_n^2 \theta_{sx}^2 r + 2(y_s \theta_{sz} - z_s \theta_{sy})k - \dfrac{2}{n}(m_y y_s + m_z z_s)\theta_{sx} r \\[2mm]
\qquad - \dfrac{2}{n}[(m_y + (nc + ph)z_s)\theta_{sz} - (m_z - (nc + ph)y_s)\theta_{sy}]\theta_{sx} q
\end{cases} \tag{2}
$$

where $\bar{\theta}_{sy} = \dfrac{2}{nr_n^2}[\dfrac{1}{d} + (\bar{y}_s^2 + \bar{z}_s^2)r][m_y + (nc + ph)\bar{z}_s]$, $\bar{\theta}_{sz} = \dfrac{2}{nr_n^2}[\dfrac{1}{d} + (\bar{y}_s^2 + \bar{z}_s^2)r][m_z - (nc + ph)\bar{y}_s]$, $\bar{y}_s = \dfrac{f_y + m_y \theta_{sx} e}{na + pe}$, and $\bar{z}_s = \dfrac{f_z + m_z \theta_{sx} e}{na + pe}$.

Moreover, these nonlinear and analytical models (Eq. (1)) can be used to deal with the more general basic multi-beam

4

modules with more generalized beams by modifying the scalar coefficients, *a, b, c, d, e, g, h, i, j, k, q, r* and s based on the work in [32] and using $\delta=G/(Ea_0)$. Here, a generalized beam with characteristic length L (overall length) is a lumped-compliance beam composed of two identical uniform compliant segments separated by one rigid segment [32], and a_0 denotes the normalized length of each compliant segment. $a_0=0.5$ is the case of distributed-compliant wire beam.

The primary motion stiffness of the basic multi-beam module increases with the increase of the number of wire beams without affecting the maximal allowable motion range. In addition, with the increase of the pitch-circle radius, all the rotational angles decrease without affecting the transverse displacements.

It is noted that, due to the symmetry of the cross section, Eq. (1) can be used to deal with the basic multi-beam module with square/round cross-sections in the following diverse layouts with the same pitch-circle radius and the same remaining conditions (see Fig. 4 for the basic four-beam module example with square cross sections).
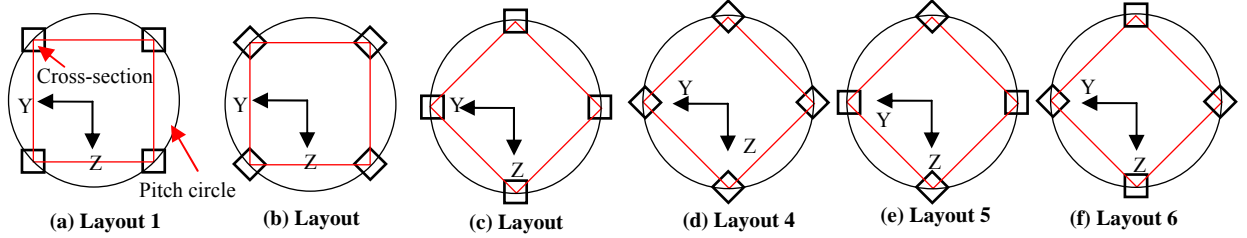
(a) Layout 1   **(b) Layout**   **(c) Layout**   **(d) Layout 4**   **(e) Layout 5**   **(f) Layout 6**

Fig. 4. Top views of the square cross-section layouts in basic four-beam modules with the same pitch-circle radius

3. Composite Multi-Beam Modules

In this section, we will investigate the load-displacement equations for composite multi-beam modules (Fig. 2). For any two composite multi-beam modules with the same inner and outer pitch-circle radii but different layouts (Fig. 5), they have the same analytical models based on the results in Fig. 4. Note that the Y- and Z-axes in the composite 2*n*-beam module are set up to be the same as those in the above basic *n*-beam module.

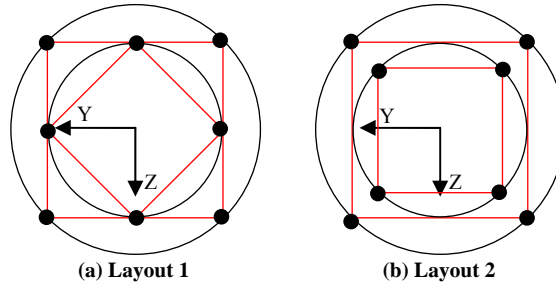**(a) Layout 1**   **(b) Layout 2**

Fig. 5. Top view for a composite four-beam module with two basic four-beam modules connected either serially or in parallel

3.1. Nonlinear analytical modeling of serial double multi-beam modules

3.1.1. Case composed of two basic three-beam modules

Considering the serial double three-beam module (i.e. composite six-beam module) on the right-hand side in Fig. 2b, let θ_{sx1}, θ_{sy1}, θ_{sz1}, x_{s1}, y_{s1}, z_{s1} be the displacement components of the motion stage with regard to the global coordinate system O-XYZ, which results from the inner basic three-beam module deformation alone, θ_{sx2}, θ_{sy2}, θ_{sz2}, x_{s2}, y_{s2}, z_{s2} be the displacements of the secondary stage with regard to the local coordinate system O'-X'Y'Z', which results from the outer basic three-beam module deformation alone.

From Eq. (1), we have

$$\theta_{sx1} \approx \frac{m_x + (m_z f_z + m_y f_y)e/(3a+pe)}{3(\delta + ar_3^2 + per_3^2/3)},\tag{3}$$

$$y_{s1} \approx \frac{f_y + m_y\theta_{sx1}e}{3a+pe},\tag{4}$$

$$z_{s1} \approx \frac{f_z + m_z\theta_{sx1}e}{3a+pe},\tag{5}$$

$$\theta_{sy1} \approx \frac{2}{3r_3^2}(\frac{1}{d} + y_{s1}^2 r + z_{s1}^2 r)[m_y + (3c+ph)z_{s1}] - 2i\theta_{sx1}y_{s1},\tag{6}$$

$$\theta_{sz1} \approx \frac{2}{3r_3^2}(\frac{1}{d} + y_{s1}^2 r + z_{s1}^2 r)[m_z - (3c+ph)y_{s1}] - 2i\theta_{sx1}z_{s1},\tag{7}$$

$$x_{s1} \approx \frac{p}{3d} + (y_{s1}^2 + z_{s1}^2)i + \frac{p}{3}(y_{s1}^2 + z_{s1}^2)r + r_3^2\theta_{sx1}^2 i + \frac{p}{3}r_3^2\theta_{sx1}^2 r + 2(y_{s1}\theta_{sz1} - z_{s1}\theta_{sy1})k - \frac{2}{3}(m_y y_{s1} + m_z z_{s1})\theta_{sx1}r \qquad (8)$$

where r_3 is the radius of the pitch circle around which the three inner beams are uniformly spaced.

We use the resultant moments acting on the secondary stage in the deformed configuration to further obtain the following:

$$\theta_{sx2} \approx \frac{-m_x + \dfrac{e}{3a - pe}[(m_z + f_y - py_{s1})f_z + (-m_y + f_z - pz_{s1})(-f_y)]}{3(\delta + ar_3'^2 - per_3'^2/3)} = \frac{-[m_x - \dfrac{e}{3a - pe}(m_z f_z + m_y f_y + (f_y m_z - f_z m_y)\dfrac{pe\theta_{sx1}}{3a + pe})]}{3(\delta + ar_3'^2 - per_3'^2/3)}, \qquad (9)$$

$$y_{s2} \approx \frac{-f_y + (-m_y + f_z - pz_{s1})\theta_{sx2}e}{3a - pe}, \qquad (10)$$

$$z_{s2} \approx \frac{f_z + (m_z + f_y - py_{s1})\theta_{sx2}e}{3a - pe}, \qquad (11)$$

$$\theta_{sy2} \approx \frac{2}{3r_3'^2}(\frac{1}{d} + y_{s2}^2 r + z_{s2}^2 r)[-m_y + f_z - pz_{s1} + (3c - ph)z_{s2}] - 2i\theta_{sx2}y_{s2}, \qquad (12)$$

$$\theta_{sz2} \approx \frac{2}{3r_3'^2}(\frac{1}{d} + y_{s2}^2 r + z_{s2}^2 r)[m_z + f_y - py_{s1} - (3c - ph)y_{s2}] - 2i\theta_{sx2}z_{s2}, \qquad (13)$$

$$x_{s2} \approx \frac{-p}{3d} + (y_{s2}^2 + z_{s2}^2)i + \frac{-p}{3}(y_{s2}^2 + z_{s2}^2)r + r_3'^2\theta_{sx2}^2 2i + \frac{-p}{3}r_3'^2\theta_{sx2}^2 r + 2(y_{s2}\theta_{sz2} - z_{s2}\theta_{sy2})k - \frac{2}{3}[(-m_y + f_z - pz_{s1})y_{s2} + (m_z + f_y - py_{s1})z_{s2}]\theta_{sx2}r \quad (14)$$

where r_3' is the radius of the pitch circle around which the three outer beams are uniformly spaced.

Then, we calculate the displacements of the motion stage of the serial double three-beam module as

$$\theta_{sx} = \theta_{sx1} - \theta_{sx2}, \qquad (15)$$

$$y_s = y_{s1} - y_{s2} + \theta_{sz2} \approx y_{s1} - y_{s2}, \qquad (16)$$

$$z_s = z_{s1} + z_{s2} + \theta_{sy2} \approx z_{s1} + z_{s2}, \qquad (17)$$

$$\theta_{sy} = \theta_{sy1} - \theta_{sy2}, \qquad (18)$$

$$\theta_{sz} = \theta_{sz1} + \theta_{sz2}, \qquad (19)$$

$$x_s = x_{s1} - x_{s2}. \qquad (20)$$

Substituting Eqs. (3) – (14) into Eqs. (15) – (20) accordingly, the displacements of the motion stage under applied loads can be obtained.

In the case that the twisting angle is well constrained, for example, the compliant multi-beam module is employed as either a standalone XY motion stage under a very large pitch-circle radius [17] or a building block of the translational compliant parallel manipulators [14, 15, and 22], Eqs. (15) – (20) can be simplified as

$$y_s \approx \frac{f_y}{3a + pe} + \frac{f_y}{3a - pe} = \frac{6af_y}{(3a)^2 - (pe)^2}, \qquad (21)$$

$$z_s \approx \frac{f_z}{3a + pe} + \frac{f_z}{3a - pe} = \frac{6af_z}{(3a)^2 - (pe)^2}, \qquad (22)$$

$$x_s \approx \frac{p}{3d} + \frac{(f_y^2 + f_z^2)}{(3a + ep)^2}i + \frac{p}{3}\frac{(f_y^2 + f_z^2)}{(3a + ep)^2}r - [-\frac{p}{3d} + \frac{(f_y^2 + f_z^2)}{(3a - ep)^2}i - \frac{p}{3}\frac{(f_y^2 + f_z^2)}{(3a - ep)^2}r]$$
$$= \frac{2p}{3d} - 12p\frac{(f_y^2 + f_z^2)}{[(3a)^2 - (ep)^2]^2}aei + \frac{2p}{3}\frac{(f_y^2 + f_z^2)}{[(3a)^2 - (ep)^2]^2}[(3a)^2 + (ep)^2]r \approx \frac{2p}{3d} - \frac{p}{3a}(y_s^2 + z_s^2)ei + \frac{p}{6}(y_s^2 + z_s^2)r \qquad (23)$$

$$\theta_{sy} \approx \frac{2}{3r_3'^2}[\frac{1}{d} + \frac{(f_y^2 + f_z^2)}{(3a + ep)^2}r][m_y + (3c + ph)\frac{f_z}{3a + pe}] + \frac{2}{3r_3'^2}[\frac{1}{d} + \frac{(f_y^2 + f_z^2)}{(3a - ep)^2}][m_y - f_z(1 - \frac{p}{3a + pe} + \frac{3c - ph}{3a - pe})], \qquad (24)$$

$$\theta_{sz} \approx \frac{2}{3r_3'^2}[\frac{1}{d} + \frac{(f_y^2 + f_z^2)}{(3a + ep)^2}r][m_z - (3c + ph)\frac{f_y}{3a + pe}] + \frac{2}{3r_3'^2}[\frac{1}{d} + \frac{(f_y^2 + f_z^2)}{(3a - ep)^2}][m_z + f_y(1 - \frac{p}{3a + pe} + \frac{3c - ph}{3a - pe})], \qquad (25)$$

$$\theta_{sx} \approx \frac{m_x + (m_z f_z + m_y f_y)e/(3a + pe)}{3(\delta + ar_3'^2 + per_3'^2/3)} + \frac{m_x - (m_z f_z + m_y f_y)e/(3a - pe)}{3(\delta + ar_3'^2 - per_3'^2/3)}. \qquad (26)$$

As shown in Eq. (21) or (22), the primary stiffness of the serial double three-beam module reduces to half and the motion range increases to double. Especially, the serial double three-beam module can significantly reduce the load-stiffening effect and produce reduced primary stiffness regardless of the direction of the axial force as a result. The small load-stiffening effect attributes to that the primary transverse stiffness always slightly decreases with increase of the absolute value of the axial tensile force. In addition, the serial double three-beam module can approximately eliminate the purely kinematic effect upon its axial displacement as the transverse forces imposed on the secondary motion stage produce positive axial displacement, while the transverse forces imposed on the motion stage produce negative axial displacement. In the case that the axial force is equal to zero, there is no axial displacement.

3.1.2. Case composed of two basic *n*-beam modules

Likewise, the nonlinear analytical load-displacement equations for the serial double *n*-beam module (i.e. composite 2*n*-beam

module) can be easily deduced based on Eqs. (3) – (20) via using the analytical models (Eq. (1)) of each individual basic n-beam module instead of those of each individual basic three-beam module during the above derivation in Sec. 3.1.1. Under the assumption of very small twisting angles, similar to Eqs. (21) – (26), we can further simplify the analytical models for the serial double n-beam module as

$$
\begin{cases}
y_s \approx \dfrac{f_y}{na + pe} + \dfrac{f_y}{na - pe} = \dfrac{2naf_y}{(na)^2 - (pe)^2} \\[2mm]
z_s \approx \dfrac{f_z}{na + pe} + \dfrac{f_z}{na - pe} = \dfrac{2naf_z}{(na)^2 - (pe)^2} \\[2mm]
x_s \approx \dfrac{2p}{nd} - \dfrac{p}{na}(y_s^2 + z_s^2)ei + \dfrac{p}{2n}(y_s^2 + z_s^2)r = p[\dfrac{2}{nd} - \dfrac{2}{na}(y_s^2 + z_s^2)ei + \dfrac{1}{2n}(y_s^2 + z_s^2)r] \\[2mm]
\theta_{sy} \approx \dfrac{2}{nr_n^2}[\dfrac{1}{d} + \dfrac{(f_y^2 + f_z^2)}{(na + ep)^2}r][m_y + (nc + ph)\dfrac{f_z}{na + pe}] + \dfrac{2}{nr_n'^2}[\dfrac{1}{d} + \dfrac{(f_y^2 + f_z^2)}{(na - ep)^2}][m_y - f_z(1 - p\dfrac{f_z}{na + pe} + \dfrac{nc - ph}{na - pe})] \\[2mm]
\theta_{sz} \approx \dfrac{2}{nr_n^2}[\dfrac{1}{d} + \dfrac{(f_y^2 + f_z^2)}{(na + ep)^2}r][m_z - (nc + ph)\dfrac{f_y}{na + pe}] + \dfrac{2}{nr_n'^2}[\dfrac{1}{d} + \dfrac{(f_y^2 + f_z^2)}{(na - ep)^2}][m_z + f_y(1 - p\dfrac{f_y}{na + pe} + \dfrac{nc - ph}{na - pe})] \\[2mm]
\theta_{sx} \approx \dfrac{m_x + (m_z f_z + m_y f_y)e/(na + pe)}{n(\delta + ar_n^2 + per_n^2/n)} + \dfrac{m_x - (m_z f_z + m_y f_y)e/(na - pe)}{n(\delta + ar_n'^2 - per_n^2/n)}
\end{cases}
\tag{27}
$$

where $n=3$ or an even number greater than 3. r_n' (or r_n) is the radius of the pitch circle around which the n outer (inner) beams are uniformly spaced. The motion stage is supported by the n inner beams.

Either of the two transverse displacement equations in Eq. (27) shows that the buckling condition: $p_{crit1}=\pm na/e=\pm 10n$ occurs when the transverse stiffness becomes zero. The twisting angle equation shows the second and third buckling conditions: $p_{crit2}= -n(\delta+ar_n^2)/(er_n^2)=-[10n+n\delta/(er_n^2)]$ and $p_{crit3}=n(\delta+ar_n'^2)/(er_n'^2)=[10n+n\delta/(er_n'^2)]$ when the twisting stiffness (also torsional stiffness) becomes zero. Therefore, the buckling axial load for the serial double n-beam module is

$$|p_{crit}|= \min (|p_{crit1}|, |p_{crit2}|, |p_{crit3}|) =10n.$$

where it is shown that the buckling load depends on the transverse stiffness, i.e. $p_{crit1}=\pm 10n$. This buckling condition implies that the buckling axial load along the positive/negative direction can always induce buckling of one basic three-beam module, which builds on the assumption that m_y and m_z are quite small.

Moreover, the axial force in the three output (DOF) equations shows the load-stiffening effect. The purely kinematic term, associated with transverse motion(s), in the axial displacement vanishes due to the introduction of the secondary stage but the purely elastic and elastokinematic terms remain.

From Eq. (27), we can also conclude that if we only exert two transverse forces at the symmetric center of all beams on the motion stage, all parasitic rotational displacements, θ_{sy} and θ_{sz}, vanish. This loading action position refers to the *center of stiffness* [33] (also see Fig. 2b). In addition, if the axial force is equal to zero, Eq. (27) further reduces to

$$
\begin{cases}
y_s \approx \dfrac{2f_y}{na}; z_s \approx \dfrac{2f_y}{na}; x_s \approx 0 \\[2mm]
\theta_{sy} \approx \dfrac{2}{nr_n^2}[\dfrac{1}{d} + \dfrac{(f_y^2 + f_z^2)}{(na)^2}r](m_y - \dfrac{f_z}{2}) + \dfrac{2}{nr_n'^2}[\dfrac{1}{d} + \dfrac{(f_y^2 + f_z^2)}{(na)^2}](m_y - \dfrac{f_z}{2}) = (\dfrac{2}{nr_n^2} + \dfrac{2}{nr_n'^2})[\dfrac{1}{d} + \dfrac{(f_y^2 + f_z^2)}{(na)^2}r](m_y - \dfrac{f_z}{2}) \\[2mm]
\theta_{sz} \approx \dfrac{2}{nr_n^2}[\dfrac{1}{d} + \dfrac{(f_y^2 + f_z^2)}{(na)^2}r](m_z + \dfrac{f_y}{2}) + \dfrac{2}{nr_n'^2}[\dfrac{1}{d} + \dfrac{(f_y^2 + f_z^2)}{(na)^2}](m_z + \dfrac{f_y}{2}) = (\dfrac{2}{nr_n^2} + \dfrac{2}{nr_n'^2})[\dfrac{1}{d} + \dfrac{(f_y^2 + f_z^2)}{(na)^2}r](m_z + \dfrac{f_y}{2}) \\[2mm]
\theta_{sx} \approx \dfrac{m_x + (m_z f_z + m_y f_y)/(10n)}{n(\delta + ar_n^2)} + \dfrac{m_x - (m_z f_z + m_y f_y)/(10n)}{n(\delta + ar_n'^2)}
\end{cases}
\tag{28a}
$$

If $r_n'=r_n$, Eq. (28a) reduces to

$$
\begin{cases}
y_s \approx \dfrac{2f_y}{na}; z_s \approx \dfrac{2f_y}{na}; x_s \approx 0 \\[2mm]
\theta_{sy} \approx \dfrac{4}{nr_n^2}[\dfrac{1}{d} + \dfrac{1}{4}(y_s^2 + z_s^2)r](m_y - \dfrac{f_z}{2}) \\[2mm]
\theta_{sz} \approx \dfrac{4}{nr_n^2}[\dfrac{1}{d} + \dfrac{1}{4}(y_s^2 + z_s^2)r](m_z + \dfrac{f_y}{2}) \\[2mm]
\theta_{sx} \approx \dfrac{2m_x}{n(\delta + ar_n^2)}
\end{cases}
\tag{28b}
$$

Note that the tiny purely kinematic and elastokinematic effects involving rotations can be further added into the axial displacement in the case of the axial force being very small. For example, if we take the purely kinematic effect from the product of transverse motion and bending rotation into account, the general form of the axial displacement can be modified as

$$
x_s \approx p[\dfrac{2}{nd} - \dfrac{2}{na}(y_s^2 + z_s^2)ei + \dfrac{1}{2n}(y_s^2 + z_s^2)r] + k(y_s\theta_{sz} - z_s\theta_{sy})
\tag{28c}
$$

If the serial double n-beam modules are used independently as a planar motion stage, the only large twisting moment acting on motion stage doesn't cause the parasitic axial displacement as long as two the pitch-circle radii are equal. A CAD prototype of serial double four-beam module in this case is shown in Fig. 6. Although, different beam lengths for the inner four beams

and the outer four beams with different circle radii can be employed to produce no axial displacement under pure twisting moment, but will negatively result in extra kinematic effect contributing to the axial displacement under pure transverse force.

In addition, there are other variations of composite multi-beam modules with secondary stages, each of which is composed of multiple (such as three or four) basic multi-beam modules connected serially to increase the motion range, as discussed in [29]. Their analytical modeling can be easily done by following the process of the above load-displacement modeling.
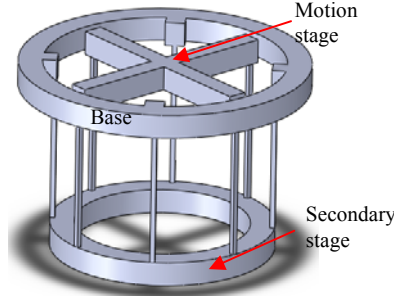
Fig. 6. A CAD model of the serial double four-beam module with two equal pitch-circle radii: $r_4'=r_4$

3.2. Analytical modeling of parallel double multi-beam modules

3.2.1. Case composed of two basic three-beam modules

Following the approximate nonlinear analytical modeling for the basic three-beam module in [16], we can obtain the load-displacement equations for the parallel double three-beam module (i.e. composite six-beam module) on the left-hand side in Fig. 2c based on the detailed derivation shown in Appendix A.1.

$$\begin{cases} \theta_{sx} \approx \dfrac{m_x + (m_z f_z + m_y f_y)e/(6a+pe)}{6[\delta + \dfrac{a}{2}(r_3^2 + r_3'^2) + \dfrac{pe(r_3^2 + r_3'^2)}{12} - \dfrac{(r_3^2 - r_3'^2)^2 \theta_{sx}^2 ie}{12(\dfrac{1}{3d} + \dfrac{y_s^2 + z_s^2}{3}r + \dfrac{r_3^2 + r_3'^2}{6}\theta_{sx}^2 r)}]} \\[4ex] y_s \approx \dfrac{f_y + m_y \theta_{sx} e}{6a + pe} \\[3ex] z_s \approx \dfrac{f_z + m_z \theta_{sx} e}{6a + pe} \\[3ex] \theta_{sy} \approx \dfrac{2}{3(r_3^2 + r_3'^2)}(\dfrac{1}{d} + y_s^2 r + z_s^2 r)[m_y + (6c + ph)z_s] - 2\theta_{sx} y_s i \\[3ex] \theta_{sz} \approx \dfrac{2}{3(r_3^2 + r_3'^2)}(\dfrac{1}{d} + y_s^2 r + z_s^2 r)[m_z - (6c + ph)y_s] - 2\theta_{sx} z_s i \\[3ex] x_s \approx \dfrac{p}{6d} + (y_s^2 + z_s^2)i + \dfrac{p}{6}(y_s^2 + z_s^2)r + \dfrac{(r_3^2 + r_3'^2)}{2}\theta_{sx}^2 i + \dfrac{p}{6}\dfrac{(r_3^2 + r_3'^2)}{2}\theta_{sx}^2 r + 2(y_s\theta_{sz} - z_s\theta_{sy})k - \dfrac{1}{3}(m_y y_s + m_z z_s)\theta_{sx} r \end{cases} \quad (29)$$

where r_3 and r_3' are the radii of the pitch circles around which the three inner beams and the three outer beams are uniformly spaced, respectively. This equation is also applicable to the parallel double three-beam module on the right-hand side in Fig. 2c.

From the twisting angle equation in Eq. (29), we can learn that the twisting stiffness increases with the increase of the twisting angle due to the introduction of the additional term (positive): $-(r_3^2 - r_3'^2)^2 ie\theta_{sx}^2 /[2(\dfrac{1}{3d} + \dfrac{y_s^2 + z_s^2}{3}r + \dfrac{r_3^2 + r_3'^2}{6}\theta_{sx}^2 r)]$ in the denominator in comparison with the twisting angle equation of the basic six-beam module (Eq. (1)). The additional term is caused by the axial displacement compatibility for the inner three-beam module and the outer three-beam module since the two individual basic three-beam modules used separately with different pitch-circle radii produce different axial displacements for the same twisting rotation.

The nonlinear twisting stiffness can be further derived as follows:

$$\frac{\partial m_x}{\partial \theta_{sx}} = 6[\delta + \frac{a}{2}(r_3^2 + r_3'^2) + \frac{pe(r_3^2 + r_3'^2)}{12}] - \frac{3(r_3^2 - r_3'^2)^2 ie}{2(\dfrac{1}{3d} + \dfrac{y_s^2 + z_s^2}{3}r + \dfrac{r_3^2 + r_3'^2}{6}\theta_{sx}^2 r)}\theta_{sx}^2 - \frac{(r_3^2 - r_3'^2)^2 (r_3^2 + r_3'^2)ier}{3(\dfrac{1}{3d} + \dfrac{y_s^2 + z_s^2}{3}r + \dfrac{r_3^2 + r_3'^2}{6}\theta_{sx}^2 r)^2}\theta_{sx}^4. \quad (30)$$

The larger both d and $(r_3^2 - r_3'^2)^2$ are, the larger the twisting stiffness nonlinearity is. In addition, the transverse motions, y_s and z_s, affect the nonlinear twisting stiffness. Specifically, the increase of the transverse motion decreases the twisting stiffness nonlinearity slightly if d is small enough. If d is larger, the contribution from the transverse motion becomes larger. Furthermore, if r_3 approaches to r_3', Eq. (30) reduces to the nonlinear equation of the basic six-beam module approximately.

3.2.2. Case composed of two basic *n*-beam modules

Based on the results in Sections 3.2.1, the load-displacement equations of the parallel double *n*-beam module (composite 2*n*-

beam module) can be deduced as follows:

$$\begin{cases} \theta_{sx} \approx \dfrac{m_x + (m_z f_z + m_y f_y)e/(2na+pe)}{2n[\delta + \dfrac{a}{2}(r_n^2 + r_n'^2) + \dfrac{pe(r_n^2 + r_n'^2)}{4n} - \dfrac{(r_n^2 - r_n'^2)^2 \theta_{sx}^2 ie}{4n(\dfrac{1}{nd} + \dfrac{y_s^2 + z_s^2}{n}r + \dfrac{r_n^2 + r_n'^2}{2n}\theta_{sx}^2 r)}]} \\[4mm] y_s \approx \dfrac{f_y + m_y \theta_{sx} e}{2na + pe} \\[3mm] z_s \approx \dfrac{f_z + m_z \theta_{sx} e}{2na + pe} \\[3mm] \theta_{sy} \approx \dfrac{2}{n(r_n^2 + r_n'^2)}(\dfrac{1}{d} + y_s^2 r + z_s^2 r)[m_y + (2nc + ph)z_s] - 2\theta_{sx} y_s i \\[3mm] \theta_{sz} \approx \dfrac{1}{n(r_n^2 + r_n'^2)}(\dfrac{1}{d} + y_s^2 r + z_s^2 r)[m_z - (2nc + ph)y_s] - 2\theta_{sx} z_s i \\[3mm] x_s \approx \dfrac{p}{2nd} + (y_s^2 + z_s^2)i + \dfrac{p}{2n}(y_s^2 + z_s^2)r + \dfrac{(r_n^2 + r_n'^2)}{2}\theta_{sx}^2 i + \dfrac{p}{2n}\dfrac{(r_n^2 + r_n'^2)}{2}\theta_{sx}^2 r + 2(y_s \theta_{sz} - z_s \theta_{sy})k - \dfrac{1}{n}(m_y y_s + m_z z_s)\theta_{sx} r \end{cases}$$ (31)

where r_n' (or r_n) is the radius of the pitch circle around which the n outer (or inner) beams are uniformly spaced. if r_n approaches to r_n', it reduces to the nonlinear equation of the basic $2n$-beam module approximately.

Equation (31) also shows that there are load-stiffening effects in the three output (DOF) equations (y_s, z_s, and θ_{sx}) and the buckling conditions can be obtained by setting up the transverse motion stiffness and/or twisting stiffness to be zero, which leads to $p_{crit} = -20n$ if θ_{sx} is small enough. It deserves to mention again that this buckling condition works if m_y and m_z are quite small.

It is shown that the axial force in the three output (DOF) equations contributes to the load-stiffening effect. Note that the parallel double n-beam module has also a stiffness center at which the transverse force act with minimized parasitic bending angles.

In addition, there are other variations of parallel double multi-beam modules, which will be discussed and modeled in Appendices A.2 and A.3. Especially, a parallel double multi-beam module can consist of two same basic multi-beam modules in a *mirror-symmetrical* configuration (see the parallel double three-beam module in Fig. 7 for example, where the two basic three-beam modules are placed in different sides from the motion stage). As it will be shown in Appendix A.3, this system has a significant load-stiffening effect under large-range translational motion, resulting from the augmentation of transverse stiffness with the increase of motion displacement in the presence of gradually increased axial tension-force in the configuration of two mirror-symmetrical three-beam modules. Here, this load-stiffening effect significantly increases a) the primary motion stiffness, which may lead to the use of only small motion linear actuators such as PZT actuators, and b) the tensile stress, which may cause yield under large-range of motion. However, the stiffness center in the parallel double three-beam module in the mirror-symmetrical configuration is at the center of the motion stage, which results in no parasitic rotation/translation under transverse forces and/or twisting moment.
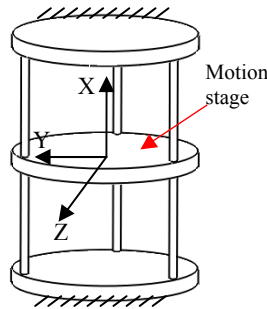

Fig. 7. Parallel double three-beam module in a symmetrical configuration

3.3 FEA comparisons

In order to measure the accuracy of the above derived analytical models and verify the correctness of the deduced models for a compliant n-beam module, FEA results are pursued to compare with the analytical models. Here, commercial software, COMSOL, is selected for nonlinear FEA using tetrahedral element and finest meshing with others default.

Firstly, we pick up the composite eight-beam modules to compare their analytical models with FEA results of the primary transverse displacement for different cases. Let the material be a standard AL6061-T651 with the Young's Modules of 69 GPa, and Poisson ratio of 0.33. The wire beam has square cross sections with thickness of 2 mm. The length of all identical wire beams is 50 mm, and the radii for the pitch circles around which the beams distribute are $R_4'=25$ mm and $R_4=20$mm for the serial double four-beam module, and $R_4'=25$ mm and $R_4=20$ mm for the parallel double four-beam module. Both Figs. 8 and 9 show that the analytical results (Eqs. (27) and (31)) of the transverse displacement along the Y-axis for both composite cases are very close to the corresponding FEA results.
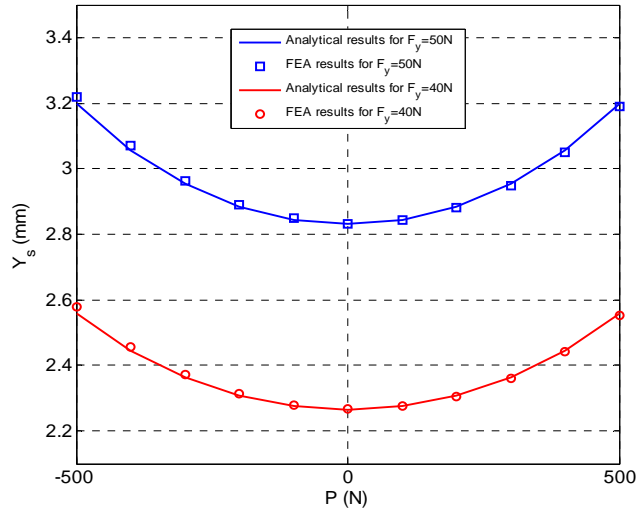
Fig. 8. Transverse displacement comparison for the serial double four-beam module
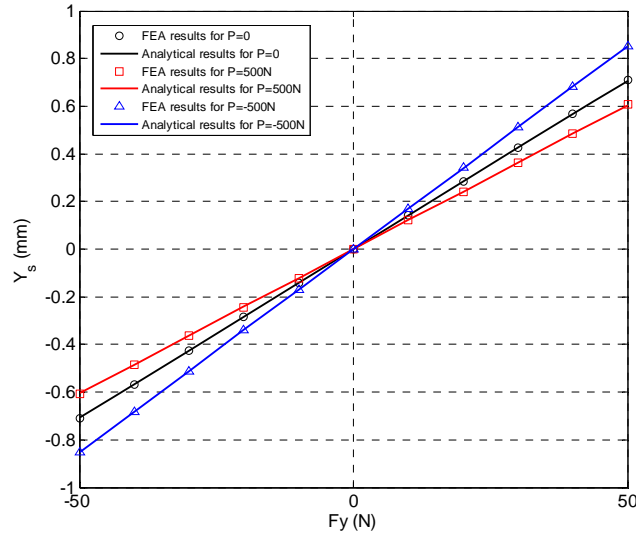

Fig. 9. Transverse displacement comparison for the parallel double four-beam module

Secondly, the double parallel three module is further chosen for verifying its twisting angle equation. Let all the beams have round cross sections of diameter D=0.5mm with length of L=5 mm, distributing round two circles with radii: R_3=5 mm or 25mm, and R_3'=50 mm. The other conditions for material are kept the same as those in the above example. Figure 10 shows a very good agreement in twisting rotation for the second case between the analytical results (Eq. (30)) and FEA results with a small difference less than 5.5%.
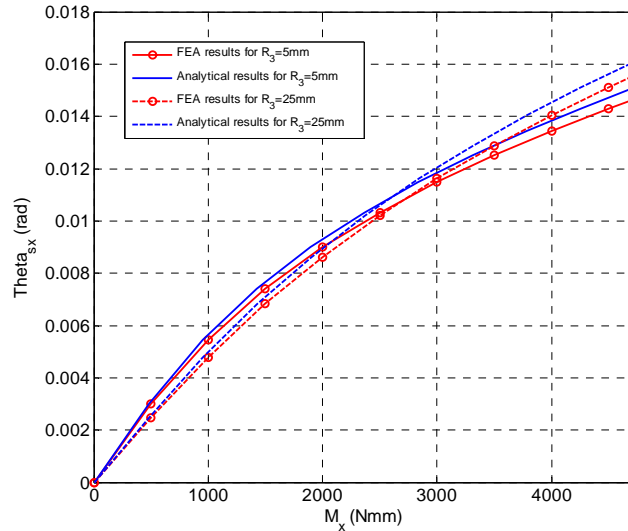
Fig. 10. Twisting rotation

4. Analytical Characteristic Analysis and Comparisons

In this section, detailed characteristic analysis and comparisons will be carried out for three types of compliant multi-beam modules with the same total beam number such as the basic six-beam module, (denoted by I-module, Fig. 2a), serial double three-beam module (denoted by II-module, Fig. 2b) and the parallel double three-beam module (denoted by III-module, Fig. 2c). We will focus on two particular applications for the three compliant six-beam modules whose twisting angles are well constrained: (a) the standalone XY motion stages under the large pitch-circle radius [17], and (b) the compositional units of translational compliant parallel manipulators [14, 15, and 22].

Let the three types of compliant six-beam modules be composed of identical beams with d=20000 and δ=1/(1+0.33)=0.7519 and also have the same overall size, i.e. the outer pitch-circle radii are same.

1) Motion range

Primary motion range of the I- II- and III-modules for both applications are approximately Δ, 2Δ and Δ. The II-module has the largest motion range, 2Δ.

2) Ratio of twisting stiffness to transverse stiffness

For the application as a standalone XY motion stage, the pitch-circle radius must be large enough (in desktop-size) compared to the beam length in order to well constrain the twisting angle. We specify the following with p=0:

$$\begin{cases} r_6 = 10 \text{ for I - module} \\ r_3 = r_3' = 10 \text{ for II - module} \\ r_3' = 10 \text{ for III - module} \end{cases}.$$

where these values of the pitch-circle radii will be adopted for other stiffness analysis for the application as the standalone XY motion stage.

Using the values of radii given above, the ratio of the twisting stiffness to the transverse stiffness for each compliant six-beam module is derived using Eqs. (1), (27) and (31) as follows:

$$\frac{\partial m_x}{\partial \theta_{sx}} / (6a)|_I = \frac{6(\delta + ar_6^2)}{6a}|_{r_6=10} = (0.7519 + 12 \times 100)/12 \approx 100, \tag{32a}$$

$$\frac{\partial m_x}{\partial \theta_{sx}} / (1.5a)|_{II} = \frac{1.5(\delta + 12r_3^2)}{1.5a}|_{r_3=r_3'=10} = (0.7519 + 12 \times 100)/12 \approx 100, \tag{32b}$$

$$\frac{\partial m_x}{\partial \theta_{sx}} / (6a)|_{III} = \{6[\delta + \frac{a}{2}(r_3^2 + r_3'^2) + \frac{pe(r_3^2 + r_3'^2)}{12}] - \frac{3(r_3^2 - r_3'^2)^2 ie}{2(\frac{1}{3d} + \frac{y_s^2 + z_s^2}{3}r)}\theta_{sx}^2\}/72|_{r_3'=10}$$

$$= \frac{6[0.7519 + 6(100 + r_3^2)] + 3.24 \times [1/(1/d + (y_s^2 + z_s^2)r)](100 - r_3^2)^2 \theta_{sx}^2}{72} > 50 \tag{32c}$$

Note that, in comparison with Eq. (31), some high-order terms associated with twisting angle in Eq. (32c) have been left out since they are trivial to the twisting stiffness calculation under a very small twisting rotation.
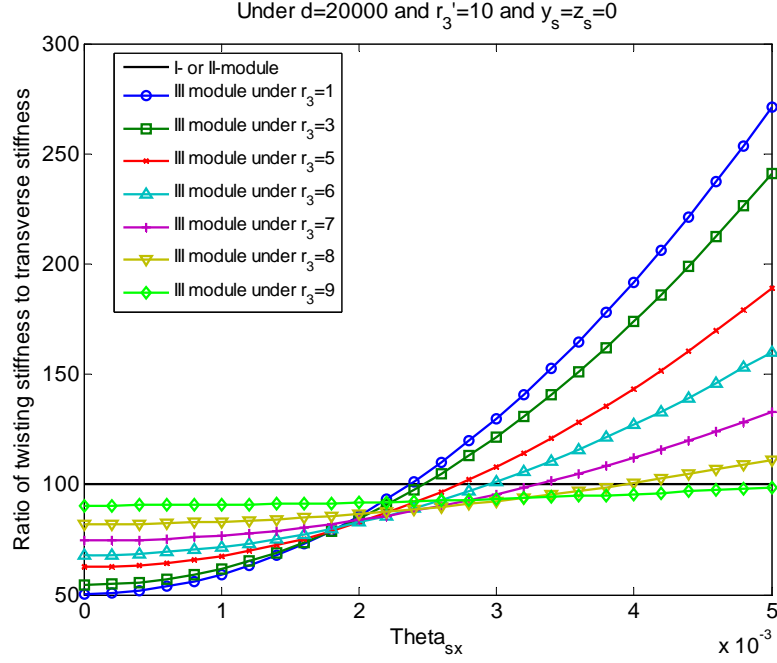
Figure 11 shows that the comparisons of the ratio of the twisting stiffness to the transverse stiffness for the application as the standalone XY motio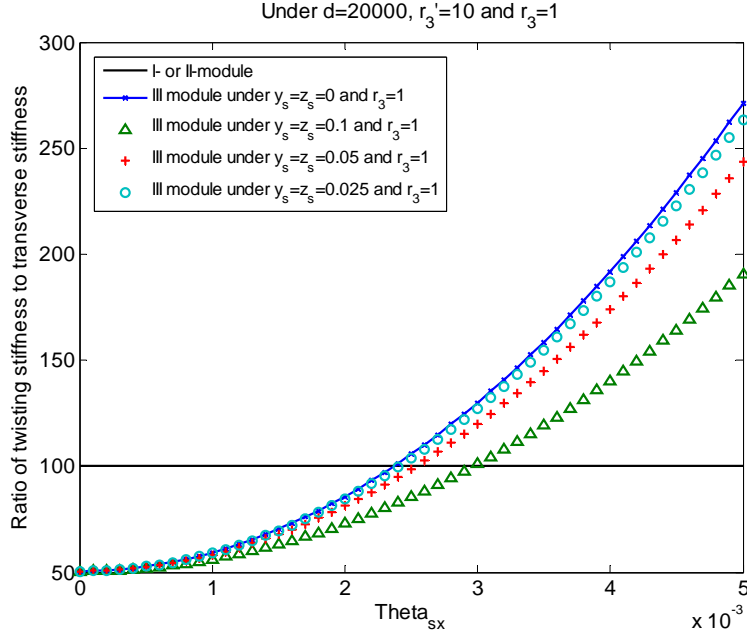n stage under no transverse motion among three compliant six-beam modules. The stiffness ratios for the I- and II-modules have the same values with a constant 100 (Eqs. (32a) and (32b)). But the stiffness ratio of the III-module has a variable value which increases with the twisting angle's increase (Eq. (32c)). The smaller r_3 is, the more significant the nonlinearity is. However, when r_3 in the III-module is the smallest, the stiffness ratio at zero point of the twisting angle is 50, half of that of the I- or II-module, while when r_3 approach r_3', the stiffness ratio at the zero point of the twisting angle is approaching to 100. Therefore, the determination of r_3 depends on the actual requirements about the initial stiffness ratio or the twisting angle at the nonlinear stiffness ratio equal to 100. Figure 12 illustrates that the increasing transverse motion reduces the ratio of the twisting stiffness to the transverse stiffness. It can be found that the effect from the transverse motion below 0.025 in both directions is negligible.

Compared with the I- or II-module, the III-module has the better twisting stiffness characteristic (nonlinear stiffening) in the case as the XY motion stage.

For the application as a compositional unit of translational compliant parallel manipulators, the twisting angle is generally to be lower than 0.001 if the transverse motion is up to 0.1, i.e. the 0.01 times smaller than the transverse motion, and the pitch-circle radius should be compatible to the beam length, so we specify the following with p=0:

$$\begin{cases} r_6 = 1 \text{ for I - module} \\ r_3 = r_3' = 1 \text{ for II - module} \\ r_3' = 1 \text{ for III - module} \end{cases}.$$

where these values of the pitch-circle radii will be adopted for other following stiffness analysis for the application as a compositional unit of translational compliant parallel manipulators.

Using the values of radii given above, the ratio of the twisting stiffness to the transverse stiffness for each module is derived accordingly as follows using Eqs. (1), (27) and (31):

$$\frac{\partial m_{\mathrm{x}}}{\partial \theta_{\mathrm{sx}}}/(6a)|_{\mathrm{I}}=\frac{6(\delta+ar_6^2)}{6a}|_{r_6=1}=(0.7519+12\times1)/12=1.0627,\tag{33a}$$

$$\frac{\partial m_{\mathrm{x}}}{\partial \theta_{\mathrm{sx}}}/(1.5a)|_{\mathrm{II}}=\frac{1.5(\delta+12r_3^2)}{1.5a}|_{r_3=r_{3'}=1}=(0.7519+12\times100)/12=1.0627,\tag{33b}$$

$$\frac{\partial m_{\mathrm{x}}}{\partial \theta_{\mathrm{sx}}}/(6a)|_{\mathrm{III}}=\frac{6[0.7519+6(1+r_3^2)]+3.24\times20000(1-r_3^2)^2\theta_{\mathrm{sx}}^2}{72}|_{r_{3'}=1}\approx[0.7519+6(1+r_3^2)]/12\leq1.0627\tag{33c}$$

Note that the twisting stiffness (Eqs. (33a), (33b) and (33c)) is trivial compared to the corresponding bending stiffness.

Fig. 11. The ratio of the twisting stiffness to the transverse stiffness for the application as an XY motion stage under no transverse motion

Fig. 12. The ratio of twisting stiffness to transverse stiffness for the application as an XY motion stage under existing transverse displacements

3) Transverse motion stiffness with load-stiffening effect

For both applications mentioned above, the transverse motion stiffness can be obtained as follows using Eqs. (1), (27) and (31) and plotted in Fig. 13.

$$\frac{\partial f_{\mathrm{y}}}{\partial y_{\mathrm{s}}}|_{\mathrm{I}}=6a+pe,\tag{34a}$$

12

$$\frac{\partial f_y}{\partial y_s}|_{\mathrm{II}} = \frac{(3a)^2 - (pe)^2}{6a}\,, \tag{34b}$$

$$\frac{\partial f_y}{\partial y_s}|_{\mathrm{III}} = 6a + pe\,. \tag{34c}$$
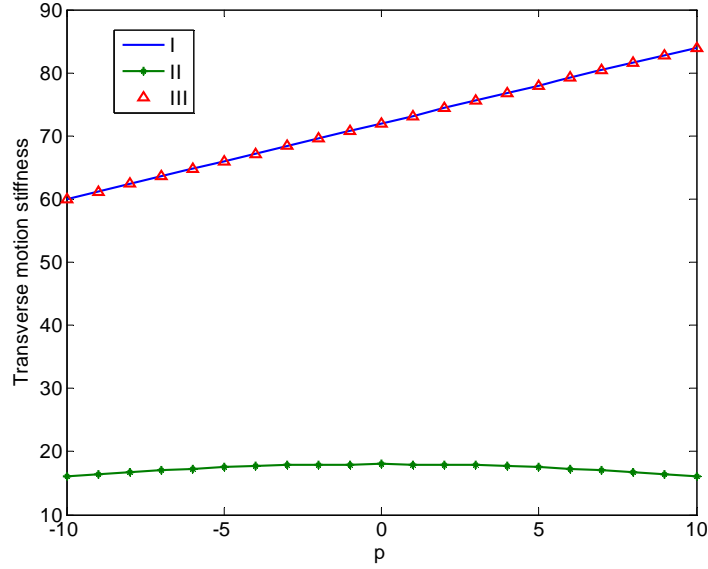
Fig. 13. Transverse stiffness with load-stiffening effect for both applications

Figure 13 shows the transverse stiffness changes with the axial force which contributes to the load-stiffening effect. With the increase of the magnitude of the axial force, the transverse stiffness decreases slightly (load-softening effect) in the II module. However, with the increase of the positive axial force, the transverse stiffness increases dramatically in the I- and III-modules. It is noted that at $p=0$, the transverse stiffness of the II-module is one quarter of that of the I-/III-module. The lowest transverse stiffness of the II-module will facilitate the use of voice coil actuator for large-range motion.

Therefore, among the three types of compliant six-beam modules, the II-module has a better characteristic in the minimized load-stiffening effect of the transverse motion for both applications, and is well suitable for the mirror-symmetrical design for large-range motion.

4) Axial displacement

For both applications under the well-constrained twisting angle, the axial displacements under $p=0$ are obtained using Eqs. (1), (27) and (31) as

$$x_s|_{\mathrm{I}} = (y_s^2 + z_s^2)i\,, \tag{35a}$$

$$x_s|_{\mathrm{II}} = 0\,, \tag{35b}$$

$$x_s|_{\mathrm{III}} = (y_s^2 + z_s^2)i\,. \tag{35c}$$

The axial displacement is herein the parasitic translational motion. The comparisons among three compliant six-beam modules for the axial displacement are shown in Fig. 14. It is physically observed that the axial displacement in the I- and III-modules has a significant increase in magnitude if the transverse motion has a large increment. As a result, the II-module has a better axial displacement characteristic for both applications.

5) Ratio of axial stiffness to transverse stiffness

For both applications under the well-constrained twisting angle, the ratio of axial stiffness to transverse stiffness for each module under $p=0$ is derived from Eqs. (1), (27) and (31) as

$$\frac{\partial p}{\partial x_s}/(6a)|_{\mathrm{I}} = 1/[\frac{1}{6d} + \frac{(y_s^2 + z_s^2)r}{6}]/(6a)\,, \tag{36a}$$

$$\frac{\partial p}{\partial x_s}/(1.5a)|_{\mathrm{II}} = 1/[\frac{2}{3d} - \frac{(y_s^2 + z_s^2)ei}{3a} + \frac{(y_s^2 + z_s^2)r}{6}]/(1.5a)\,, \tag{36b}$$

$$\frac{\partial p}{\partial x_s}/(6a)|_{\mathrm{III}} = 1/[\frac{1}{6d} + \frac{(y_s^2 + z_s^2)r}{6}]/(6a)\,. \tag{36c}$$

Figure 15 illustrates that the ratio of axial stiffness to transverse stiffness goes down over the primary motion range $[-0.1, 0.1]$. It is shown that the II-module has the worst ratio of the axial stiffness to the transverse stiffness with significant decrease over the primary motion in comparison with those of the I- and III-modules. The loss in the axial stiffness in the II-module is caused by the internal in-plane DOFs induced by the secondary stage.
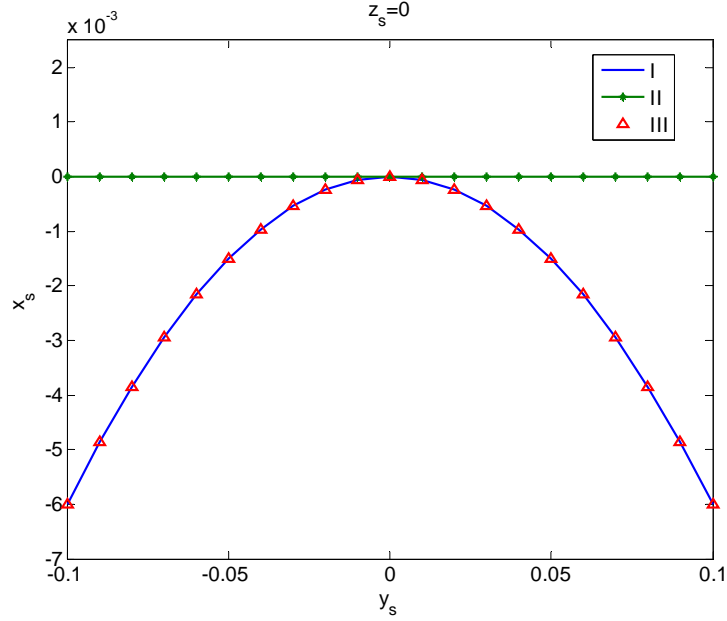
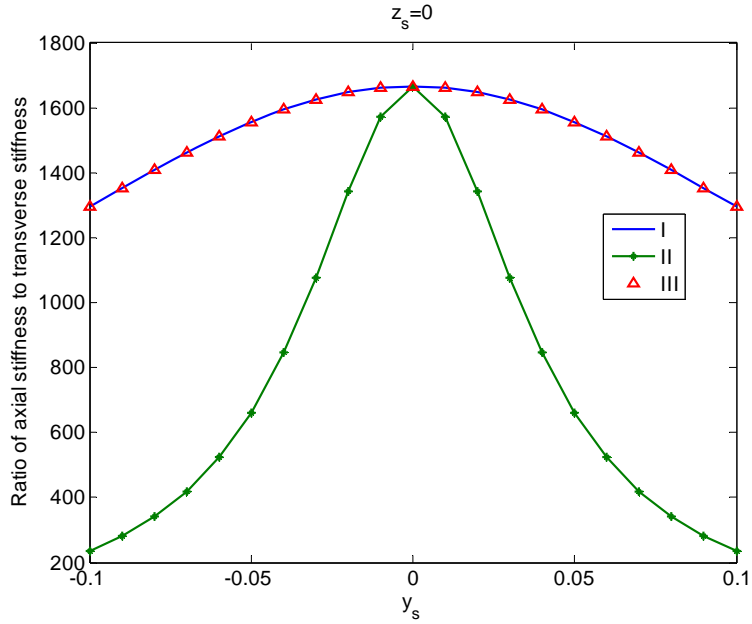**Fig. 14.** Axial displacement for both applications

Fig. 15. Ratio of the axial stiffness to the transverse stiffness for both applications

6) Ratio of bending stiffness to transverse stiffness

For the application as a standalone XY motion stage under $p=0$, the ratio of bending stiffness (about the Y- or Z-axis) to transverse stiffness for each module is obtained based on Eqs. (1), (27) and (31) as follows

$$\frac{\partial m_y}{\partial \theta_{sy}}/(6a)\Big|_{\mathrm{I}} = 1/[\frac{2}{6\times r_6^2}(\frac{1}{d}+(y_s^2+z_s^2)r)]/6a\Big|_{r_6=10} = 1/[\frac{2}{6\times 100}(\frac{1}{20000}+\frac{y_s^2+z_s^2}{700})]/72, \tag{37a}$$

$$\frac{\partial m_y}{\partial \theta_{sy}}/(1.5a)\Big|_{\mathrm{II}} = 1/[\frac{4}{3\times r_3^2}(\frac{1}{d}+\frac{(y_s^2+z_s^2)r}{4})]/(1.5a)\Big|_{r_3=r_3'=10} = 1/[\frac{4}{3\times 100}(\frac{1}{20000}+\frac{y_s^2+z_s^2}{2800})]/18, \tag{37b}$$

$$\frac{\partial m_y}{\partial \theta_{sy}}/(6a)\Big|_{\mathrm{III}} = 1/[\frac{2}{3\times(r_3^2+r_3'^2)}(\frac{1}{d}+(y_s^2+z_s^2)r)]/(6a)\Big|_{r_3'=10} = 1/[\frac{2}{3\times(100+r_3^2)}(\frac{1}{20000}+\frac{y_s^2+z_s^2}{700})]/72. \tag{37c}$$

It is shown from Fig. 16 that the ratio of bending stiffness to the transverse stiffness goes down over the primary motion range. The II-module has the best stiffness ratio of bending stiffness to transverse stiffness, and the III-module has the approximately same stiffness ratio of bending stiffness to transverse stiffness as that of the I-module if r_3 is close to r_3'.
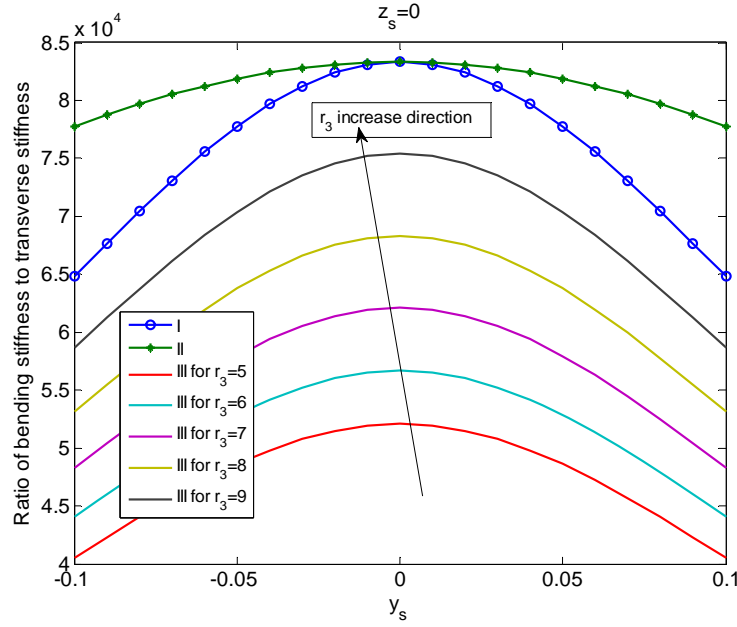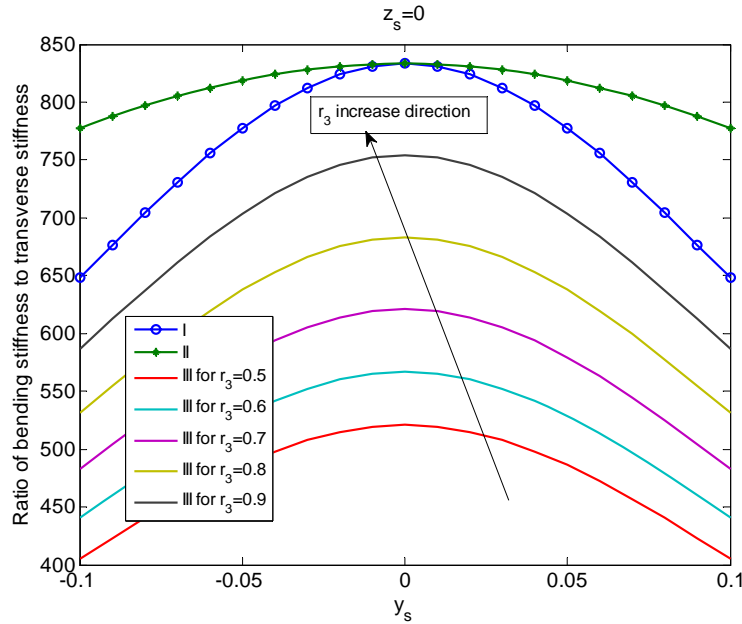
Fig. 16. Ratio of bending stiffness to transverse stiffness for the XY motion stage application (color difference can be seen in the electronic version)

For the applications as a compositional unit of translational compliant parallel manipulators under $p=0$, the ratio of bending stiffness (about each axis) to the transverse motion stiffness for each module with the help of Eqs. (1), (27) and (31) is shown as

$$\frac{\partial m_y}{\partial \theta_{sy}}/(6a)\,|_{\mathrm{I}} = 1/[\frac{2}{6\times r_6^2}(\frac{1}{d}+(y_s^2+z_s^2)r)]/6a\,|_{r_6=1} = 1/[\frac{2}{6\times 1}(\frac{1}{20000}+\frac{y_s^2+z_s^2}{700})]/72\,, \tag{38a}$$

$$\frac{\partial m_y}{\partial \theta_{sy}}/(1.5a)\,|_{\mathrm{II}} = 1/[\frac{4}{3\times r_3^2}(\frac{1}{d}+\frac{(y_s^2+z_s^2)r}{4})]/(1.5a)\,|_{r_3=r_3'=1} = 1/[\frac{4}{3\times 1}(\frac{1}{20000}+\frac{y_s^2+z_s^2}{2800})]/18\,, \tag{38b}$$

$$\frac{\partial m_y}{\partial \theta_{sy}}/(6a)\,|_{\mathrm{III}} = 1/[\frac{2}{3\times(r_3^2+r_3'^2)}(\frac{1}{d}+(y_s^2+z_s^2)r)]/(6a)\,|_{r_3'=1} = 1/[\frac{2}{3\times(1+r_3^2)}(\frac{1}{20000}+\frac{y_s^2+z_s^2}{700})]/72\,. \tag{38c}$$

Similarly, the II-module has the best stiffness ratio of bending stiffness to transverse stiffness (Fig. 17).

Fig. 17. Ratio of bending stiffness to transverse stiffness for the compositional unit application (color difference can be seen in the electronic version)

7) Buckling load

From Eqs. (1), (27) and (31), it is obtained that the buckling loads of the I-, II-, and III-modules for both applications are 60, 30, and 60, respectively. The I- and III-modules have the largest buckling load, 60.

15

8) Dynamics

The II-module has an under-constrained secondary stage/mass with three planar DOFs, and only behaves well under quasi-static/low speed motion mode. The non-controllable mass would lead to uncontrolled vibrations in high-speed motion, which negatively affect dynamic performance. However, the I-/III-module is the exact-constrained design.

9) Summary

Tables 1 and 2 summarize the above characteristic analysis results for the three types of compliant six-beam modules. The I-module possesses the simplest configuration. The II-module has the largest motion range, smallest primary motion stiffness and load-stiffening effect, smallest parasitic axial displacement, and largest bending stiffness ratio while it also has the worst axial stiffness ratio, buckling load, and dynamic performance. The III-module has the nonlinear twisting stiffness characteristics and larger axial stiffness. Therefore, the compliant multi-beam modules should be chosen based on the actual characteristics requirements in specific applications.

It is noted when the compliant multi-beam module is used as a compositional unit, the transverse stiffness with load-stiffening effect may also contribute to the cross-axis coupling, the parasitic axial displacement can also contribute to the cross-axis coupling and/or actuator isolation effect, and the axial stiffness can also contribute to the actuator isolation, lost motion and/or drive stiffness effect [4].

Table 1 Primary performance characteristic comparisons for the XY motion stage ('+' denoting good and '0'denotes normal/bad)

XY motion stage	Motion range	Twisting stiffness	Transverse stiffness with load-stiffening effect	Axial displacement	Axial stiffness	Bending stiffness	Buckling load	Dynamics
I-module	0	0	0	0	+	0	+	+
II-module	+	0	+	+	0	+	0	0
III-module	0	+	0	0	+	0	+	+

Table 2 Primary performance characteristic comparisons for the compositional unit of translational compliant parallel manipulators ('+' denoting good and '0' denotes normal/bad)

Compositional unit	Motion range	Twisting stiffness	Transverse stiffness with load-stiffening effect	Axial displacement	Axial stiffness	Bending stiffness	Buckling load	Dynamics
I-module	0	0	0	0	+	0	+	+
II-module	+	0	+	+	0	+	0	0
III-module	0	0	0	0	+	0	+	+

In addition, the following observations can be made for the compliant multi-beam modules:
(1) The out-of-plane stiffness of the motion stage decreases with the increase of the transverse motion.
(2) The out-of-plane load, such as axial force p, changes the in-plane motion stiffness of the motion stage.

5. Discussions

From the initial FEA results about the translational compliant parallel manipulators using compliant multi-beam modules as the building blocks, it has been found that the bending normal stress is the dominant factor associated with yield as compared with other tensile normal stress and/or shear stress. Here, the beams in the compliant multi-beam modules can be regarded as guided beams (zero end slopes). Because the compliant multi-beam modules can achieve translations along two directions, it is desired to investigate which type of symmetrical cross-section of guided beams can produce the maximal single-axis translation or the maximal two-axis translations (considering the bending normal stress superposition of two-axis bending) and identify where the maximal stress positions are for the single-axis bending and two-axis bending.

There are many other options to optimize/improve the compliant multi-beam modules. These options could be non-identical beams, lumped compliance as opposed to distributed compliance, asymmetric cross sections, non-parallel beams, and slaving of secondary motion stages etc.

6. Conclusions

Nonlinear modeling and analytical characteristic analysis of compliant multi-beam modules have been investigated in this paper for enabling rapid characteristic analysis and design synthesis. The main contributions are:
1) Nonlinear load-displacement equations have been derived and deduced for the composite multi-beam modules including the serial double multi-beam modules and the parallel double multi-beam modules (in non-symmetrical configuration).
2) Detailed characteristic analysis and comparisons have been undertaken for three types of compliant six-beam modules.
The present work provides a theoretical foundation for the design and nonlinear analytical modeling of the resulting *compliant manipulators* composed of compliant multi-beam modules. In addition, the work regarding the modeling and

analysis of exact-constrained compliant multi-beam modules can be beneficial to the analysis of buildings, supported by pillars, under wind loading.

The general case of error analysis for the compliant multi-beam modules is still an open issue.

Acknowledgement

References

[1] Lobontiu, N., 2002, *Compliant Mechanisms: Design of Flexure Hinges*, CRC PRESS, Boca Raton.

[2] Howell, L.L., 2001, *Compliant Mechanisms*, Wiley, New York.

[3] Howell, L.L., Maglegy, S.P., and Olsen B.M., 2013, *Handbook of Compliant Mechanism*s, Wiley, New York.

[4] Awtar, S., and Slocum, A.H., 2007, "Constraint-Based Design of Parallel Kinematic XY Flexure Mechanisms", *Journal of Mechanical Design*, 129 (8):816-830.

[5] Dai, J.S., Ding, X.L., 2006, "Compliance Analysis of a Three-Legged Rigidly-Connected Platform Device", *Journal of Mechanical Design*, 128 (6): 755–764.

[6] Samuel, H.D. and Sergio, N.S., 1979, *Compliant Assembly System*, United States Patent, No. 4155169.

[7] Hale, L.C., 1999, "*Principles and Techniques for Designing Precision Machines*", PhD thesis, Massachusetts Institute of Technology, Cambridge, MA

[8] Su, H.-J., Dorozhkin, D. V., and Vance, J. M., 2009, "A Screw Theory Approach for the Conceptual Design of Flexible Joints for Compliant Mechanisms", *Journal of Mechanisms and Robotics*, 1(4): 041009.

[9] Su, H.-J., and Tari, H., 2010, "Realizing Orthogonal Motions With Wire Flexures Connected in Parallel", J*ournal of Mechanical Design*, 132(1): 121002

[10] Su, H.-J., and Tari, H., 2011, "On Line Screw Systems and Their Application to Flexure Synthesis", *Journal of Mechanisms and Robotics*, 3(1): 011009.

[11] Hopkins, J.B., and Culpepper, M. L., 2010, "Synthesis of Multi-Degree of Freedom, Parallel Flexure System Concepts via Freedom and Constraint Topology (FACT). Part I: Principles", *Precision Engineering*, 34(1): 259–270.

[12] Hopkins, J.B., and Culpepper, M. L., 2010, "Synthesis of Multi-Degree of Freedom, Parallel Flexure System Concepts via Freedom and Constraint Topology (FACT). Part II: Practice", *Precision Engineerin*g, 34(1):271–278.

[13] Yu, J., Li, S., Su, H.-J., and Culpepper, M.L., 2011, "Screw Theory Based methodology for the Deterministic Type Synthesis of Flexure Mechanisms", *Journal of Mechanisms and Robotic*s, 3:031008.

[14] Hao, G., Kong, X., 2012, "Design and Modeling of a Large-Range Modular XYZ Compliant Parallel Manipulator Using Identical Spatial Modules", *Journal of Mechanism and Robotics*, 4 (2):021009-1-021009-10.

[15] Hao, G., 2013, "Towards the Design of Monolithic Decoupled XYZ Compliant Parallel Mechanisms for Multi-function Applications", *Mechanical Sciences*, 4:291-302.

[16] Hao, G., Kong, X., and Reuben, L.L., 2011, "A Nonlinear Analysis of Spatial Compliant Parallel Modules: Multi-Beam Modules", *Mechanism and Machine Theory*, 46 (5):680-706.

[17] Hao, G., 2013, "Simplified PRBMs of Spatial Compliant Multi-beam Modules for Planar Motion", *Mechanical Sciences*, 4:311-318.

[18] Hao, G., Kong, X., 2013, "A Normalization-Based Approach to the Mobility Analysis of Spatial Compliant Multi-Beam Modules", *Mechanism and Machine Theory*, 59(5):1-19.

[19] Culpepper, M.L., Magleby, S.P., Howell, L.L., DiBiasio, C.M., and Panas, R.M., 2011, "*Carbon Nanotube Based Compliant Mechanism*", US Patent, No. US7884525B2.

[20] Howell, L.L., DiBiasio, C.M., Cullinan, M.A., Panas, R. and Culpepper, M.L, 2010, "A Pseudo-Rigid-Body Model for Large Deflections of Fixed-Clamped Carbon Nanotubes", *Journal of Mechanisms and Robotics*, 2(3): 034501.

[21] Culpepper, M., DiBiasio C., Panas R., Magleby S., and Howell, L.L., 2006, "Simulation of a Carbon Nanotube-based Compliant Parallel-guiding Mechanism: A Nanomechanical Building Block", *Applied Physical Letters*, 89: 203111.

[22] Hao, G., and Kong, X., 2012, "Novel XY Compliant Parallel Manipulators for Large Translation with Enhanced Out-of-Plane Stiffness", *Journal of Mechanical Design*, 134: 061009.

[23] Awtar, S., Ustick, J., and Sen, S., 2012, "An XYZ Parallel Kinematic Flexure Mechanism with Geometrically Decoupled Degrees of Freedom", *ASME Journal of Mechanisms and Robotics*, 5(1):015001

[24] Pham, H.-H., Yeh, H. C., Chen, I.-M., 2006, "Micromanipulation System Design Based on Selective Actuation Mechanisms", *The International Journal of Robotics Research*, 25(2): 171–185.

[25] Sen, S., and Awtar, S., 2012, "A Closed-Form Non-linear Model for the Constraint Characteristics of Symmetric Spatial Beams", *ASME Journal of Mechanical Design*, 135(3): 031003

[26] Sen, S., and Awtar, S., 2010, "Nonlinear Constraint Model for Symmetric Three-Dimensional Beams", *Proceedings of the ASME 2010 International Design Engineering Technical Conferences &Computers and Information in Engineering Conference*, August 15–18, 2010, Montreal, Quebec, Cananda. DETC2010-28953

[27] Ramirez, I.A., and Lusk, C.P., 2011, "Spatial-Beam Large-Deflection Equations and Pseudo-Rigid-Body Model for Axisymmetric Cantilever Beams", *Proceedings of the ASME 2011 International Design Engineering Technical*

Conferences &Computers and Information in Engineering Conference, August 29–31, 2011, Washington, DC, US. DETC2011-47389

[28] Awtar, S., and Parmar, G., 2012, "Design of a Large Range XY Nanopositioning System", *ASME Journal of Mechanisms and Robotics*, 5(2):021008.

[29] Hao, G., 2011, "*Creative Design and Modelling of Large-Range Translational Compliant Parallel Manipulators*", PhD Thesis, Heriot-Watt University, Edinburgh, UK.

[30] Sen, S., 2012, "*Beam Constraint Model: Generalized Nonlinear Closed-form Modeling of Beam Flexures for Flexure Mechanism Design*", Sc.D. thesis, University of Michigan.

[31] Sen, S., and Awtar, S., 2013, "Non-Linear Strain Energy Formulation of a Generalized Bisymmetric Spatial Beam for Flexure Mechanism Analysis", *ASME Journal of Mechanical Design*, 136(2): 021002.

[32] Awtar, S., and Slocum, A.H., 2007, "Characteristics of Beam-Based Flexure Modules", Journal of Mechanical Design, 129(6): 624–639.

[33] Hao, G., 2013, "A 2-legged XY Parallel Flexure Motion Stage with Minimized Parasitic Rotation", *Proceedings of the IMechE, Part C: Journal of Mechanical Engineering Science*. (In Press).

Appendix A. Nonlinear Analytical Modeling for Parallel Double Multi-beam Modules

A.1. Parallel double three-beam module

The nonlinear modeling of the parallel double three-beam module (Fig. 2c) can be derived starting from the approximate analytical solutions of the basic three-beam module (Eq. (1)). Since the displacements of the motion stage center are specified as the output displacements of the parallel double three-beam module under applied loads at this center. This center is also the specified point for the displacements (and loads) of the individual basic three-beam module. Therefore, the motion compatibility condition for two individual modules is that they have the same motion displacements denoted by x_s, y_s, z_s, θ_{sx}, θ_{sy} and θ_{sz}. We also split the loads, p, f_y, f_z, m_x, m_y and m_z, into two groups. One loading group is p_A, f_{yA}, f_{zA}, m_{xA}, m_{yA} and m_{zA} at the center contributing to the deformation of the inner basic three-beam module, and the other loading group is p_B, f_{yB}, f_{zB}, m_{xB}, m_{yB} and m_{zB} at the center contributing to the deformation of the outer basic three-beam module. The load equilibrium equations are shown below:

$$\begin{cases} p_A + p_B = p \\ f_{yA} + f_{yB} = f_y \\ f_{zA} + f_{zB} = f_z \\ m_{xA} + m_{xB} = m_x \\ m_{yA} + m_{yB} = m_y \\ m_{zA} + m_{zB} = m_z \end{cases} . \tag{A.1}$$

The load-displacements equations for each individual basic three-beam module can be written as

$$\begin{cases} m_{xA} + (m_{zA}z_s + m_{yA}y_s)e = 3\theta_{sx}(\delta + ar_3^2 + p_A er_3^2/3) \\ f_{yA} + m_{yA}\theta_{sx}e = y_s(3a + p_A e) \\ f_{zA} + m_{zA}\theta_{sx}e = z_s(3a + p_A e) \\ \theta_{sy} = \frac{2}{3r_3^2}(\frac{1}{d} + y_s^2 r + z_s^2 r)[m_{yA} + (3c + p_A h)z_s] - 2\theta_{sx}y_s i \\ \theta_{sz} = \frac{2}{3r_3^2}(\frac{1}{d} + y_s^2 r + z_s^2 r)[m_{zA} - (3c + p_A h)y_s] - 2\theta_{sx}z_s i \\ x_s = \frac{p_A}{3d} + (y_s^2 + z_s^2)i + \frac{p_A}{3}(y_s^2 + z_s^2)r + r_3^2 \theta_{sx}^2 i + \frac{p_A}{3}r_3^2 \theta_{sx}^2 r + 2(y_s \theta_{sz} - z_s \theta_{sy})k - \frac{2}{3}(m_{yA}y_s + m_{zA}z_s)\theta_{sx}r \end{cases} . \tag{A.2}$$

$$\begin{cases} m_{xB} + (m_{zB}z_s + m_{yB}y_s)e = 3\theta_{sx}(\delta + ar_3^{'2} + p_B er_3^{'2}/3) \\ f_{yB} + m_{yB}\theta_{sx}e = y_s(3a + p_B e) \\ f_{zB} + m_{zB}\theta_{sx}e = z_s(3a + p_B e) \\ \theta_{sy} = \frac{2}{3r_3^{'2}}(\frac{1}{d} + y_s^2 r + z_s^2 r)[m_{yB} + (3c + p_B h)z_s] - 2\theta_{sx}y_s i \\ \theta_{sz} = \frac{2}{3r_3^{'2}}(\frac{1}{d} + y_s^2 r + z_s^2 r)[m_{zB} - (3c + p_B h)y_s] - 2\theta_{sx}z_s i \\ x_s = \frac{p_B}{3d} + (y_s^2 + z_s^2)i + \frac{p_B}{3}(y_s^2 + z_s^2)r + r_3^{'2} \theta_{sx}^2 i + \frac{p_B}{3}r_3^{'2} \theta_{sx}^2 r + 2(y_s \theta_{sz} - z_s \theta_{sy})k - \frac{2}{3}(m_{yB}y_s + m_{zB}z_s)\theta_{sx}r \end{cases} . \tag{A.3}$$

Equaling the two axial displacements in Eqs. (A.2) and (A.3), we can derive the following relation:

$$x_s = \frac{p_A}{3d} + (y_s^2 + z_s^2)i + \frac{p_A}{3}(y_s^2 + z_s^2)r + r_3^2\theta_{sx}^2 i + \frac{p_A}{3}r_3^2\theta_{sx}^2 r + 2(y_s\theta_{sz} - z_s\theta_{sy})k - \frac{2}{3}(m_{yA}y_s + m_{zA}z_s)\theta_{sx}r$$

$$= \frac{p_B}{3d} + (y_s^2 + z_s^2)i + \frac{p_B}{3}(y_s^2 + z_s^2)r + r_3'^2\theta_{sx}^2 i + \frac{p_B}{3}r_3'^2\theta_{sx}^2 r + 2(y_s\theta_{sz} - z_s\theta_{sy})k - \frac{2}{3}(m_{yB}y_s + m_{zB}z_s)\theta_{sx}r. \tag{A.4}$$

$$\Rightarrow \frac{p_A}{3d} + \frac{p_A}{3}(y_s^2 + z_s^2)r + r_3^2\theta_{sx}^2 i + \frac{p_A}{3}r_3^2\theta_{sx}^2 r \approx \frac{p_B}{3d} + \frac{p_B}{3}(y_s^2 + z_s^2)r + r_3'^2\theta_{sx}^2 i + \frac{p_B}{3}r_3'^2\theta_{sx}^2 r$$

The result of Eq. (A.4) combining the axial force equilibrium equation in Eq. (A.1) yields the axial load p_B

$$\frac{p - p_B}{3d} + \frac{p - p_B}{3}(y_s^2 + z_s^2)r + r_3^2\theta_{sx}^2 i + \frac{p - p_B}{3}r_3^2\theta_{sx}^2 r = \frac{p_B}{3d} + \frac{p_B}{3}(y_s^2 + z_s^2)r + r_3'^2\theta_{sx}^2 i + \frac{p_B}{3}r_3'^2\theta_{sx}^2 r$$

$$\Rightarrow p_B = \frac{p(\frac{1}{3d} + \frac{y_s^2 + z_s^2}{3}r + \frac{r_3^2 + r_3'^2}{6}\theta_{sx}^2 r) + (r_3^2 - r_3'^2)\theta_{sx}^2 i + p\frac{(r_3^2 - r_3'^2)}{6}\theta_{sx}^2 r}{2(\frac{1}{3d} + \frac{y_s^2 + z_s^2}{3}r + \frac{r_3^2 + r_3'^2}{6}\theta_{sx}^2 r)} \approx \frac{p}{2} + \frac{(r_3^2 - r_3'^2)\theta_{sx}^2 i}{2(\frac{1}{3d} + \frac{y_s^2 + z_s^2}{3}r + \frac{r_3^2 + r_3'^2}{6}\theta_{sx}^2 r)}. \tag{A.5}$$

Then p_A is obtained as

$$p_A = p - p_B = \frac{p}{2} - \frac{(r_3^2 - r_3'^2)\theta_{sx}^2 i}{2(\frac{1}{3d} + \frac{y_s^2 + z_s^2}{3}r + \frac{r_3^2 + r_3'^2}{6}\theta_{sx}^2 r)}. \tag{A.6}$$

Note that the derivations for p_A and p_B mainly consider the independent contribution of the twisting rotation.

After adding the two axial displacement equations in Eqs. (A.2) and (A.3) together and combining the equilibrium equations in Eq. (A.1), we have the axial displacement along the X-axis

$$2x_s = \frac{p_A}{3d} + (y_s^2 + z_s^2)i + \frac{p_A}{3}(y_s^2 + z_s^2)r + r_3^2\theta_{sx}^2 i + \frac{p_A}{3}r_3^2\theta_{sx}^2 r + 2(y_s\theta_{sz} - z_s\theta_{sy})k - \frac{2}{3}(m_{yA}y_s + m_{zA}z_s)\theta_{sx}r$$

$$+ \frac{p_B}{3d} + (y_s^2 + z_s^2)i + \frac{p_B}{3}(y_s^2 + z_s^2)r + r_3'^2\theta_{sx}^2 i + \frac{p_B}{3}r_3'^2\theta_{sx}^2 r + 2(y_s\theta_{sz} - z_s\theta_{sy})k - \frac{2}{3}(m_{yB}y_s + m_{zB}z_s)\theta_{sx}r$$

$$\Rightarrow 2x_s \approx \frac{p}{3d} + 2(y_s^2 + z_s^2)i + \frac{p}{3}(y_s^2 + z_s^2)r + (r_3^2 + r_3'^2)\theta_{sx}^2 i + \frac{p}{6}(r_3^2 + r_3'^2)\theta_{sx}^2 r - \frac{(r_3^2 - r_3'^2)^2\theta_{sx}^4 ir}{6(\frac{1}{3d} + \frac{y_s^2 + z_s^2}{3}r + \frac{r_3^2 + r_3'^2}{6}\theta_{sx}^2 r)} \tag{A.7}$$

$$+ 4(y_s\theta_{sz} - z_s\theta_{sy})k - \frac{2}{3}(m_y y_s + m_z z_s)\theta_{sx}r$$

$$\Rightarrow x_s \approx \frac{p}{6d} + (y_s^2 + z_s^2)i + \frac{p}{6}(y_s^2 + z_s^2)r + \frac{(r_3^2 + r_3'^2)}{2}\theta_{sx}^2 i + \frac{p}{6}\frac{(r_3^2 + r_3'^2)}{2}\theta_{sx}^2 r + 2(y_s\theta_{sz} - z_s\theta_{sy})k - \frac{1}{3}(m_y y_s + m_z z_s)\theta_{sx}r$$

Furthermore, the twisting displacement about the X-axis can be obtained by adding the two twisting displacement equations in both Eqs. (A.2) and (A.3) together, combining the force equilibrium equations in Eq. (A.1) and using the results in Eqs. (A.5) and (A.6):

$$m_{xA} + (m_{zA}z_s + m_{yA}y_s)e + m_{xB} + (m_{zB}z_s + m_{yB}y_s)e = 3\theta_{sx}(\delta + ar_3'^2 + p_B er_3'^2/3) + 3\theta_{sx}(\delta + ar_3^2 + p_A er_3^2/3)$$

$$\Rightarrow m_x + (m_z z_s + m_y y_s)e = 6\theta_{sx}\delta + 3a(r_3'^2 + r_3^2)\theta_{sx} + p_B er_3'^2\theta_{sx} + p_A er_3^2\theta_{sx}$$

$$\Rightarrow m_x + (m_z z_s + m_y y_s)e = 6\theta_{sx}\delta + 3a(r_3'^2 + r_3^2)\theta_{sx} \tag{A.8}$$

$$+ [\frac{p}{2} + \frac{(r_3^2 - r_3'^2)\theta_{sx}^2 i}{2(\frac{1}{3d} + \frac{y_s^2 + z_s^2}{3}r + \frac{r_3^2 + r_3'^2}{6}\theta_{sx}^2 r)}]er_3'^2\theta_{sx} + [\frac{p}{2} - \frac{(r_3^2 - r_3'^2)\theta_{sx}^2 i}{2(\frac{1}{3d} + \frac{y_s^2 + z_s^2}{3}r + \frac{r_3^2 + r_3'^2}{6}\theta_{sx}^2 r)}]er_3^2\theta_{sx}$$

$$\Rightarrow m_x + (m_z z_s + m_y y_s)e = 6\delta\theta_{sx} + 3a(r_3'^2 + r_3^2)\theta_{sx} + \frac{pe(r_3'^2 + r_3^2)}{2}\theta_{sx} - \frac{(r_3^2 - r_3'^2)^2 ie}{2(\frac{1}{3d} + \frac{y_s^2 + z_s^2}{3}r + \frac{r_3^2 + r_3'^2}{6}\theta_{sx}^2 r)}\theta_{sx}^3$$

Similarly, the transverse displacements along the Y- and Z- axes can be derived as

$$f_{yA} + m_{yA}\theta_{sx}e + f_{yB} + m_{yB}\theta_{sx}e = y_s(3a + p_B e) + y_s(3a + p_A e)$$

$$\Rightarrow f_y + m_y\theta_{sx}e = y_s(6a + pe), \tag{A.9}$$

$$f_z + m_z\theta_{sx}e = z_s(6a + pe). \tag{A.10}$$

It is noted that z_s and y_s can be represented by $f_y/(6a+pe)$ and $f_z/(6a+pe)$ in Eq. (A.8) based on the results in Eqs. (A.9) and (A.10).

The rotational displacements about the Y-axis in both Eqs. (A.2 and A.3) can be re-written as

$$\frac{\theta_{sy} + 2\theta_{sx}y_s i}{\frac{2}{3r_3'^2}(\frac{1}{d} + y_s^2 r + z_s^2 r)} = [m_{yB} + (3c + p_B h)z_s], \tag{A.11a}$$

$$\frac{\theta_{sy} + 2\theta_{sx}y_s i}{\dfrac{2}{3r_3^2}\left(\dfrac{1}{d} + y_s^2 r + z_s^2 r\right)} = [m_{yA} + (3c + p_A h)z_s] .$$ (A.11b)

The addition of Eqs. (A.11a) and (A.11b) along with the use of Eq. (A.1) gives

$$\frac{\theta_{sy} + 2\theta_{sx}y_s i}{\dfrac{2}{3r_3'^2}\left(\dfrac{1}{d} + y_s^2 r + z_s^2 r\right)} + \frac{\theta_{sy} + 2\theta_{sx}y_s i}{\dfrac{2}{3r_3^2}\left(\dfrac{1}{d} + y_s^2 r + z_s^2 r\right)} = [m_{yB} + (3c + p_B h)z_s] + [m_{yA} + (3c + p_A h)z_s]$$

$$\Rightarrow (\theta_{sy} + 2\theta_{sx}y_s i)r_3'^2 + (\theta_{sy} + 2\theta_{sx}y_s i)r_3^2 = \frac{2}{3}\left(\frac{1}{d} + y_s^2 r + z_s^2 r\right)[m_y + (6c + ph)z_s]$$ (A.12)

$$\Rightarrow (\theta_{sy} + 2\theta_{sx}y_s i)(r_3'^2 + r_3^2) = \frac{2}{3}\left(\frac{1}{d} + y_s^2 r + z_s^2 r\right)[m_y + (6c + ph)z_s]$$

Then the rotational displacement along the Y-axis is obtained as

$$\theta_{sy} = \frac{2}{3(r_3'^2 + r_3^2)}\left(\frac{1}{d} + y_s^2 r + z_s^2 r\right)[m_y + (6c + ph)z_s] - 2\theta_{sx}y_s i .$$ (A.13)

Similarly, the rotational displacement about the Z-axis is derived as follows:

$$\theta_{sz} = \frac{2}{3(r_3'^2 + r_3^2)}\left(\frac{1}{d} + y_s^2 r + z_s^2 r\right)[m_z + (6c + ph)y_s] - 2\theta_{sx}z_s i .$$ (A.14)

A.2. Variations of parallel double multi-beam modules in a non-symmetrical configuration

In this section, we will analyze other types of parallel double multi-beam modules where the number of the beams around inner pitch circle differs from that of the beams around the outer pitch circle. We will discuss a composite four-beam module and a composite nine-beam module as shown in Fig. A.1.
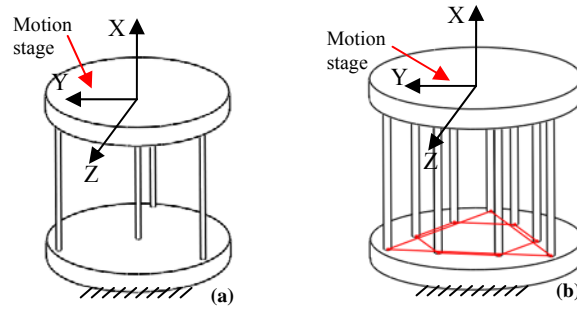
Fig. A.1. Other types of parallel double multi-beam modules: (a) composite four-beam module with three beams distributed around a regular triangle and one beam connecting to the center; (b) composite nine-beam module with the layouts that three outer beams distributed around a regular triangle and the six inner beams distributed around a regular hexagon

Following the derivation in Section A.1, the nonlinear load-displacement equations for the above composite four-beam module (Fig. A.1a) can be derived as

$$
\begin{cases}
\theta_{sx} \approx \dfrac{m_x + (m_z f_z + m_y f_y)e/(4a + pe)}{4[\delta + \frac{3}{4}ar_3^2 + \frac{3per_3^2}{16} - \dfrac{3r_3^4\theta_{sx}^2 ie}{16(1/d + y_s^2 r + z_s^2 r + r_3^2\theta_{sx}^2 r)}]} \\[4mm]
y_s \approx \dfrac{f_y + m_y\theta_{sx}e}{4a + pe} \\[3mm]
z_s \approx \dfrac{f_z + m_z\theta_{sx}e}{4a + pe} \\[3mm]
\theta_{sy} \approx \dfrac{2}{3r_3^2[\frac{2(p+bg)}{3r_3^2}(\frac{1}{d}+y_s^2 r+z_s^2 r)+1]}(\frac{1}{d}+y_s^2 r+z_s^2 r)[m_y + (4c+ph)z_s] - \dfrac{2\theta_{sx}y_s i}{\frac{2(p+bg)}{3r_3^2}(\frac{1}{d}+y_s^2 r+z_s^2 r)+1} \\[3mm]
\quad \approx \dfrac{2}{3r_3^2}(\frac{1}{d}+y_s^2 r+z_s^2 r)[m_y+(4c+ph)z_s] - 2\theta_{sx}y_s i \\[3mm]
\theta_{sz} \approx \dfrac{2}{3r_3^2[\frac{2(p+bg)}{3r_3^2}(\frac{1}{d}+y_s^2 r+z_s^2 r)+1]}(\frac{1}{d}+y_s^2 r+z_s^2 r)[m_z - (4c+ph)y_s] - \dfrac{2\theta_{sx}z_s i}{\frac{2(p+bg)}{3r_3^2}(\frac{1}{d}+y_s^2 r+z_s^2 r)+1} \\[3mm]
\quad \approx \dfrac{2}{3r_3^2}(\frac{1}{d}+y_s^2 r+z_s^2 r)[m_z-(4c+ph)y_s] - 2\theta_{sx}z_s i \\[3mm]
x_s \approx \dfrac{3p - 3[1/(1/d+y_s^2 r+z_s^2 r)]r_3^2\theta_{sx}^2 i}{12d} + (y_s^2+z_s^2)i + \dfrac{3p - 3[1/(1/d+y_s^2 r+z_s^2 r)]r_3^2\theta_{sx}^2 i}{12}(y_s^2+z_s^2)r + r_3^2\theta_{sx}^2 i \\[3mm]
\quad + \dfrac{3p - 3[1/(1/d+y_s^2 r+z_s^2 r)]r_3^2\theta_{sx}^2 i}{12}r_3^2\theta_{sx}^2 r + 2(y_s\theta_{sz} - z_s\theta_{sy})k
\end{cases}
\tag{A.15}
$$

where r_3 is the radius of the pitch circle around which the outer three beams are uniformly spaced .

From the twisting angle equation in Eq. (A.15), we can also learn that the twisting stiffness increases with the increase of the twisting angle due to the introduction of the additional term (positive), $-3r_3^4\theta_{sx}^2 ie/[4(1/d + y_s^2 r + z_s^2 r + r_3^2\theta_{sx}^2 r)]$ in the denominator.

In addtion, the nonlinear analytical model for the above composite nine-beam module (Fig. A.1b) can be obtained as

$$
\begin{cases}
\theta_{sx} \approx \dfrac{m_x + (m_z f_z + m_y f_y)e/(9a + pe)}{9[\delta + \frac{3a(r_3'^2 + 2r_6^2)}{9} + \frac{pe(r_3'^2 + 2r_6^2)}{27} - \dfrac{2(r_6^2 - r_3'^2)^2\theta_{sx}^2 ie}{9(\frac{1}{d}+(y_s^2+z_s^2)r + \frac{(2r_3'^2+r_6^2)}{3}\theta_{sx}^2 r)}]} \\[4mm]
y_s \approx \dfrac{f_y + m_y\theta_{sx}e}{9a + pe} \\[3mm]
z_s \approx \dfrac{f_z + m_z\theta_{sx}e}{9a + pe} \\[3mm]
\theta_{sy} = \dfrac{2}{3(r_3'^2 + 2r_6^2)}(\frac{1}{d}+y_s^2 r+z_s^2 r)[m_y+(9c+ph)z_s] - 2\theta_{sx}y_s i \\[3mm]
\theta_{sz} \approx \dfrac{2}{3(r_3'^2 + 2r_6^2)}(\frac{1}{d}+y_s^2 r+z_s^2 r)[m_z-(9c+ph)y_s] - 2\theta_{sx}z_s i \\[3mm]
x_s \approx \dfrac{p_B}{3d} + (y_s^2+z_s^2)i + \dfrac{p_B}{3}(y_s^2+z_s^2)r + r_3'^2\theta_{sx}^2 i + \dfrac{p_B}{3}r_3'^2\theta_{sx}^2 r + 2(y_s\theta_{sz} - z_s\theta_{sy})k
\end{cases}
\tag{A.16}
$$

where $p_B = \dfrac{p}{3} + \dfrac{2(r_6^2 - r_3'^2)\theta_{sx}^2 ie}{(\frac{1}{d}+(y_s^2+z_s^2)r + \frac{(2r_3'^2+r_6^2)}{3}\theta_{sx}^2 r)}$. r_3' is the radius of the pitch circle around which the three outer beams are uniformly spaced, and r_6 is the radius of the pitch circle around which the six inner beams are uniformly spaced.

A.3. Parallel double three-beam module in a symmetrical configuration

Consider the parallel double three-beam module in a symmetrical configuration shown in Fig. 7. If there is only one transverse force, f_y, acting at the center of the motion stage, there will be only a resulting transverse displacement, y_s, with the other displacements of zero values at the motion stage center.

Based on Eq. (1), configuration symmetry property and the above intuitive analysis results, we have

$$
y_s = \dfrac{f_y/2}{3a + p'e},
\tag{A.17}
$$

$$x_s = \frac{p'}{3d} + y_s^2 i + \frac{p'}{3} y_s^2 r = 0 \tag{A.18}$$

where p' is the internal tensile force (positive) caused by the primary motion.

From Eq. (A.18), we can solve for p' as

$$p' = \frac{-y_s^2 i}{\dfrac{1}{3d} + \dfrac{y_s^2 r}{3}} = \frac{0.6 y_s^2}{\dfrac{1}{3d} + \dfrac{y_s^2}{2100}}. \tag{A.19}$$

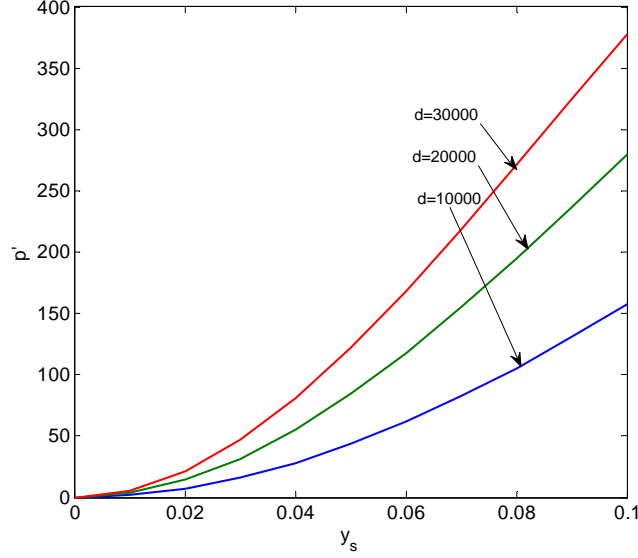The plot of p' versus y_s (over [0, 0.1]) is shown in Fig. A.2.

Fig. A.2. The tensile force versus transverse displacement in normalized values

From Fig. A.2, we can observe that the significant increase of the internal tensile force, p', with the increase of transverse displacement of y_s, which complies well with our intuitive analysis of load stiffening effect. Especially, when d increases, the tensile force becomes larger at any specified y_s.

Substituting Eq. (A.19) into Eq. (A.17), we obtain the transverse displacement as

$$y_s = \frac{f_y}{6a + 2p'e} = \frac{f_y}{72 + 2.4 \times 0.6 y_s^2 / (\dfrac{1}{3d} + \dfrac{y_s^2}{2100})}, \tag{A.20}$$

Differentiating Eq. (A.20) with regard to y_s, the transverse stiffness equation is derived as follows, which is also plotted in Fig. A.3:

$$\frac{\partial f_y}{\partial y_s} = 72 + \frac{4.32 y_s^2}{(\dfrac{1}{3d} + \dfrac{y_s^2}{2100})} - \frac{2.88 y_s^4}{2100 (\dfrac{1}{3d} + \dfrac{y_s^2}{2100})^2}. \tag{A.21}$$
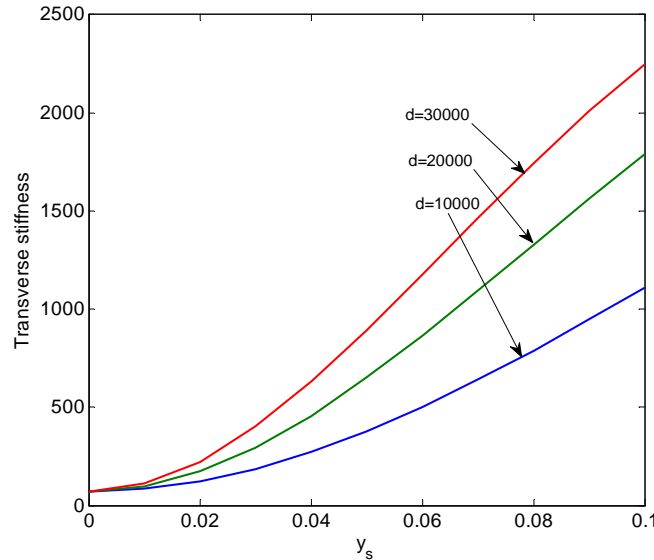
Fig. A.3. The transverse stiffness versus transverse displacement in normalized values

Figure A.3 clearly shows the load-stiffening effect that transverse stiffness, $\partial f_y / \partial y_s$, has a dramatic increase with the increase of transverse displacement of y_s and approaches to 2250 at y_s=0.1 under d=3000 in comparison with the transverse stiffness 72 at y_s=0 under d=3000. It is also seen that the load-stiffening effect becomes drastic from y_s=0.01 onwards, which indicates that this symmetrical system has approximately constant transverse stiffness within a very small motion range of 0.01. Note that the increase of d can strengthen the load-stiffening effect.
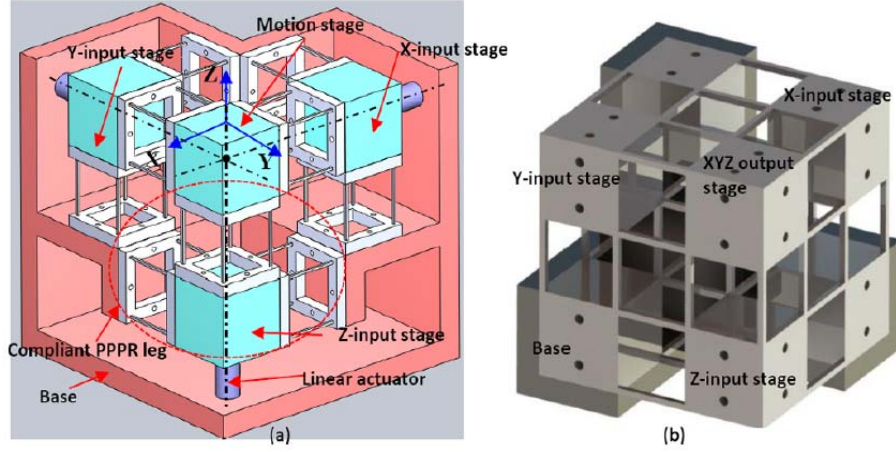
Fig. 1. A compact and decoupled XYZ compliant parallel manipulator composed of identical basic compliant four-beam modules: (a) a 3-PPPR XYZ compliant parallel manipulator, and (b) a corresponding monolithic design fabricated from a cubic material by three orthogonal directions' cutting.

(a) Type I: basic six-beam module   **(b) Type II: serial double three-beam module**   **(c) Type III: parallel double three-beam module**
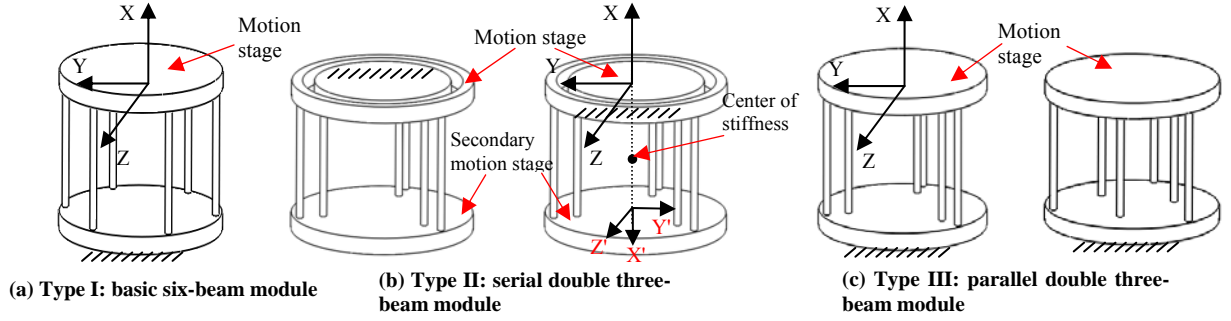
Fig. 2. Three types of compliant six-beam modules including basic and composite configurations

Fig. 3. Free body diagram of a basic three-beam module [16]
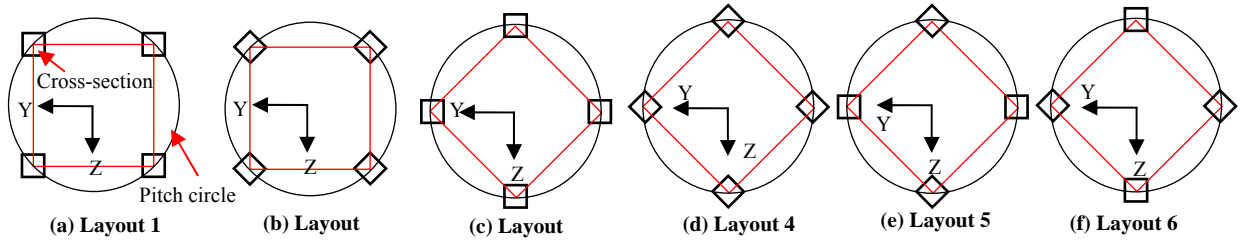
24

Fig. 4. Top views of the square cross-section layouts in basic four-beam modules with the same pitch-circle radius
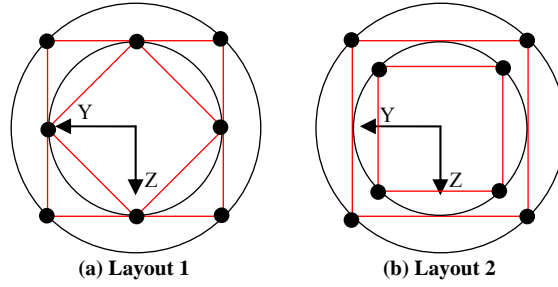
Fig. 5. Top view for a composite four-beam module with two basic four-beam modules connected either serially or in parallel
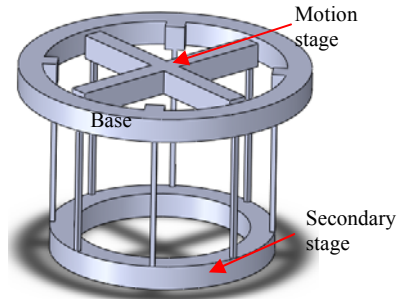
Fig. 6. A CAD model of the serial double four-beam module with two equal pitch-circle radii: $r_4'=r_4$
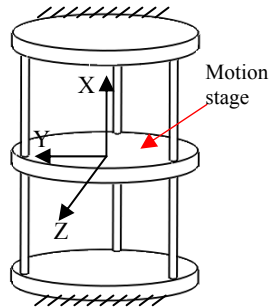
Fig. 7. Parallel double three-beam module in a symmetrical configuration
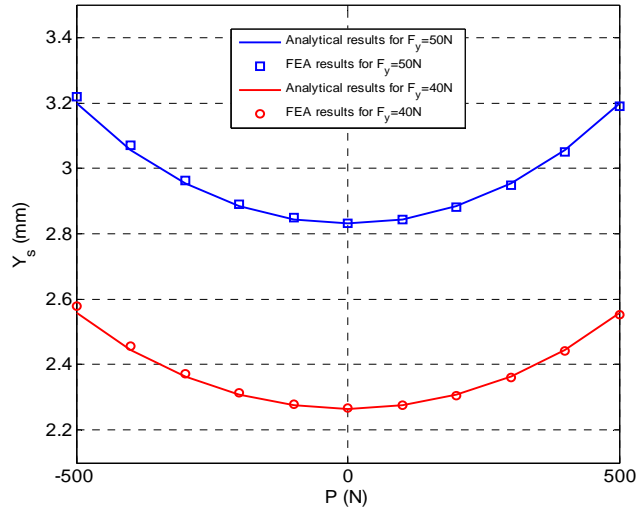
Fig. 8. Transverse displacement comparison for the serial double four-beam module
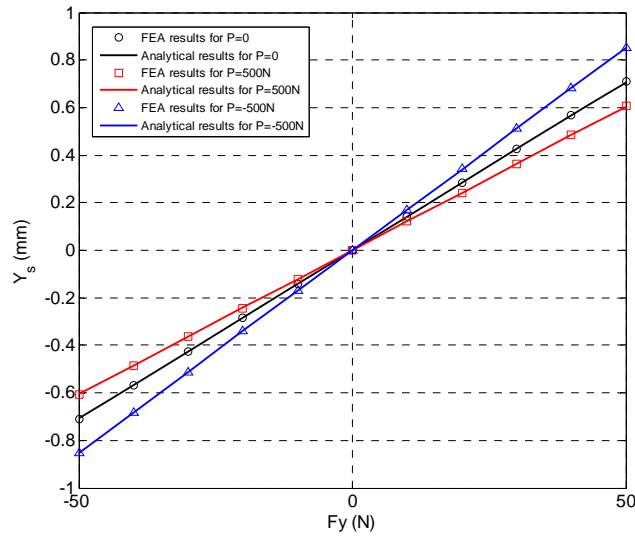
Fig. 9. Transverse displacement comparison for the parallel double four-beam module
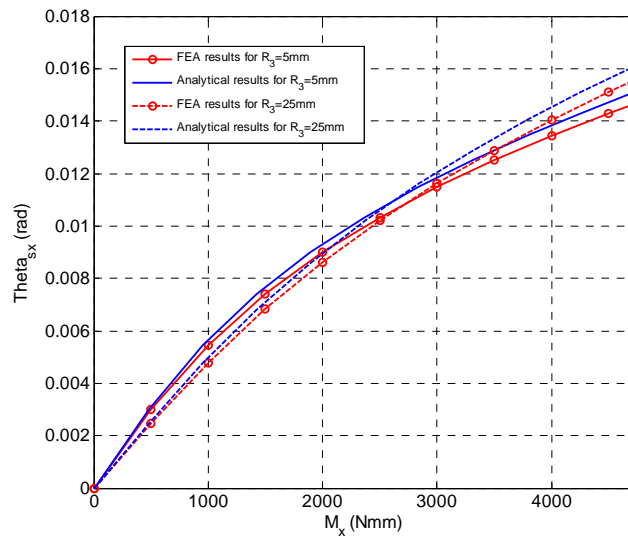
Fig. 10. Twisting rotation
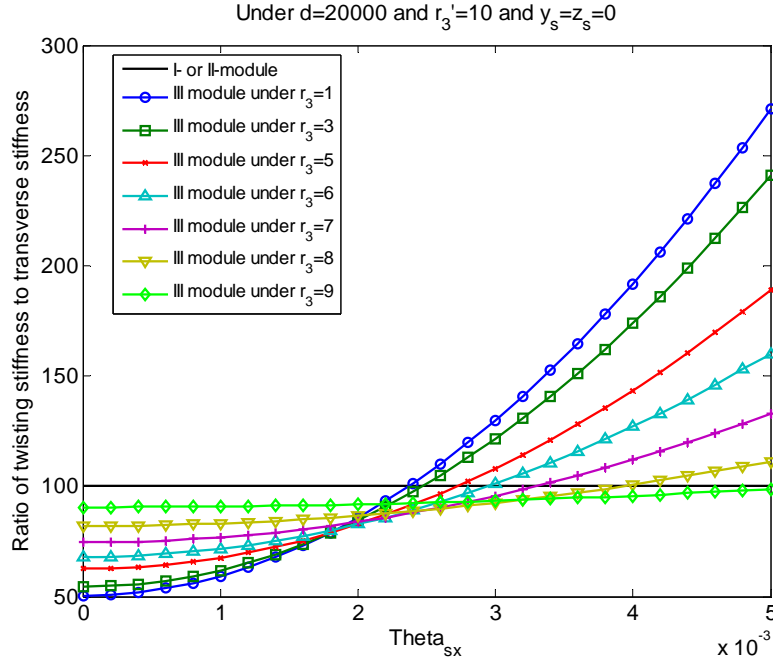
Fig. 11. The ratio of the twisting stiffness to the transverse stiffness for the application as an XY motion stage under no transverse motion
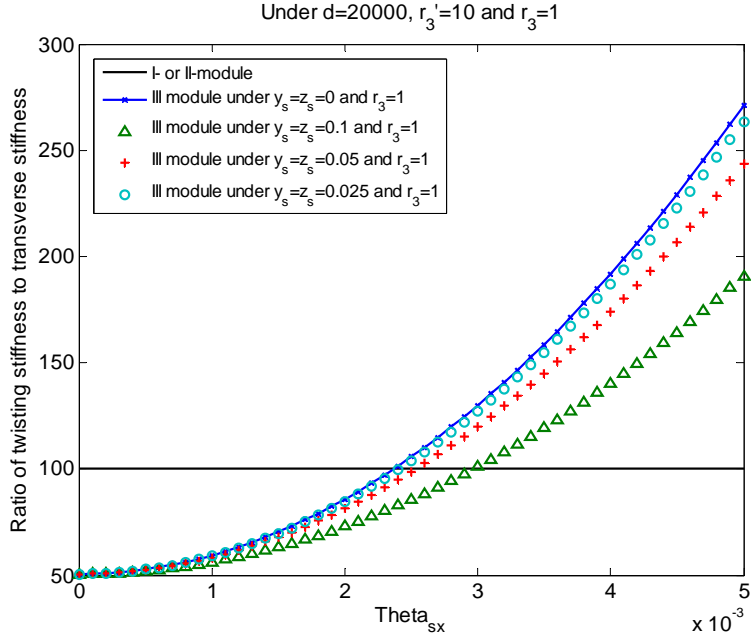
Fig. 12. The ratio of twisting stiffness to transverse stiffness for the application as an XY motion stage under existing transverse displacements
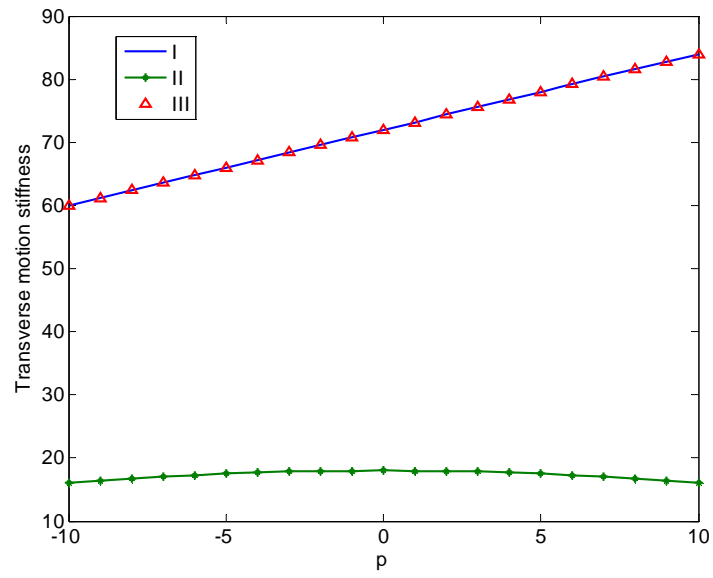
Fig. 13. Transverse stiffness with load-stiffening effect for both applications
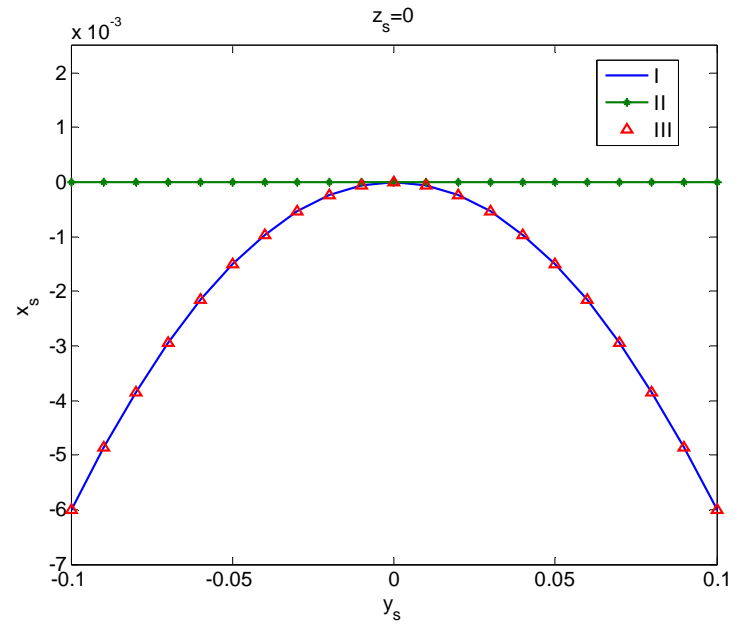
Fig. 14. Axial displacement for both applications
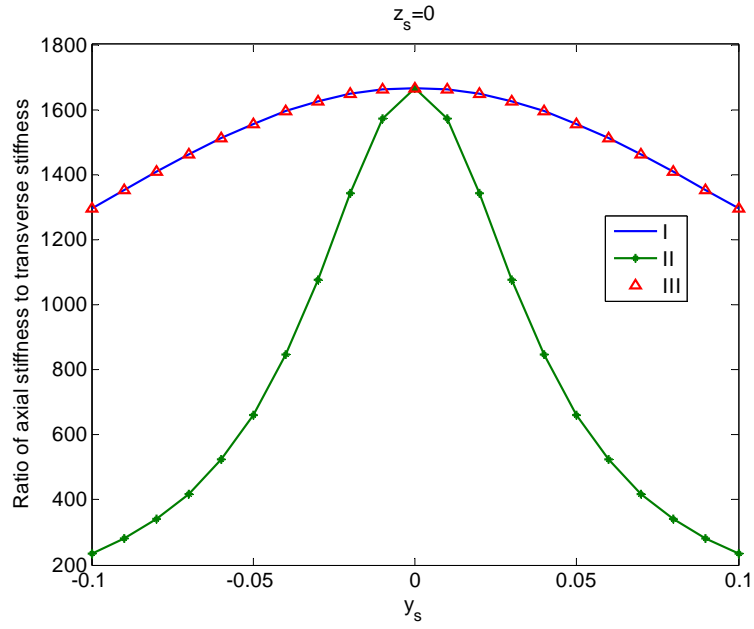
Fig. 15. Ratio of the axial stiffness to the transverse stiffness for both applications
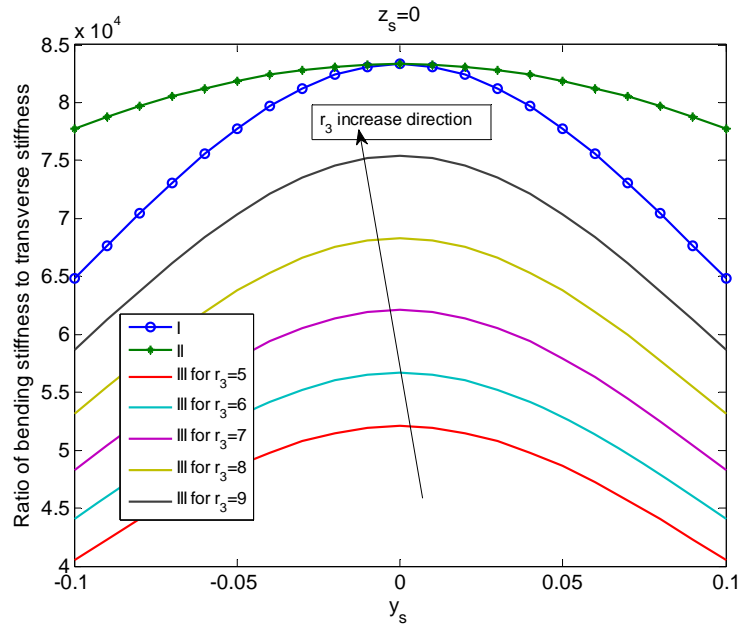
Fig. 16. Ratio of bending stiffness to transverse stiffness for the XY motion stage application (color difference can be seen in the electronic version)
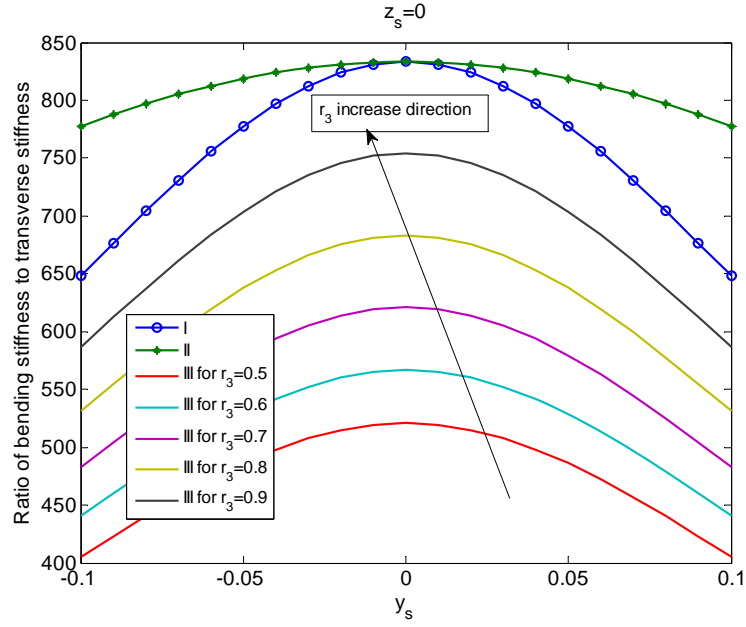
Fig. 17. Ratio of bending stiffness to transverse stiffness for the compositional unit application (color difference can be seen in the electronic version)
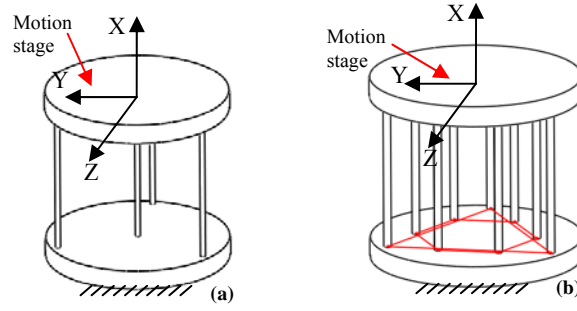

Fig. A.1. Other types of parallel double multi-beam modules: (a) composite four-beam module with three beams distributed around a regular triangle and one beam connecting to the center; (b) composite nine-beam module with the layouts that three outer beams distributed around a regular triangle and the six inner beams distributed around a regular hexagon
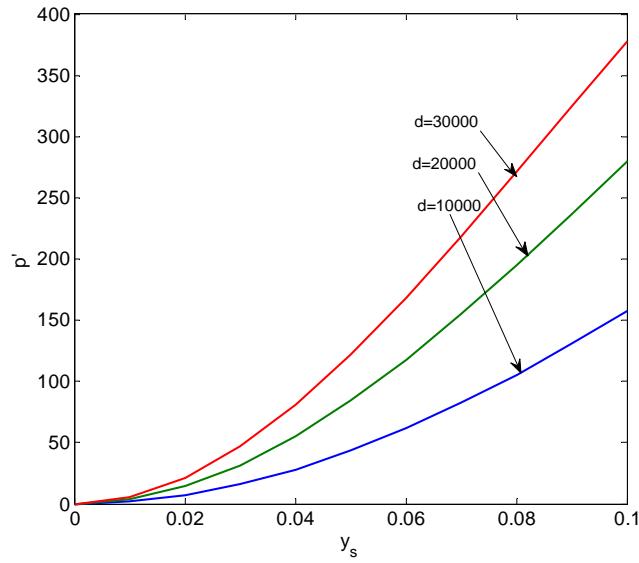

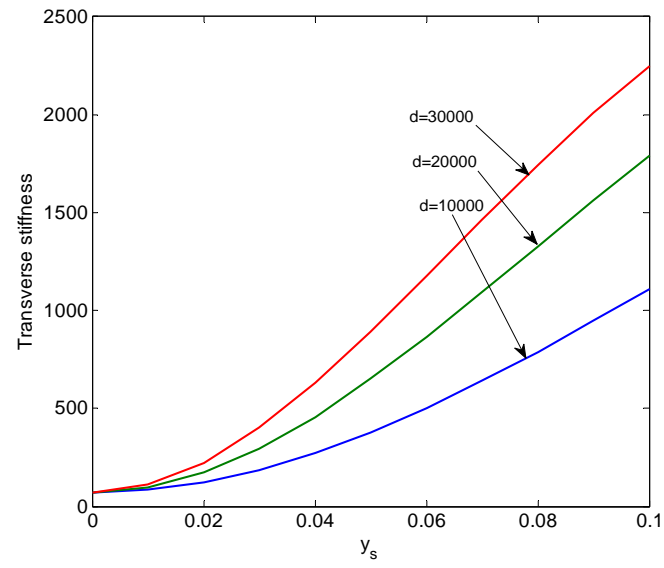**Fig. A.2.** The tensile force versus transverse displacement in normalized values

30

Fig. A.3. The transverse stiffness versus transverse displacement in normalized values